

1 **Heritability estimates of cortical anatomy: the influence and reliability of**
2 **different estimation strategies**

3 Sejal Patel^{1,2*}, Raihaan Patel^{3,4}, Min Tae M. Park^{3,5}, Mario Masellis⁶, Jo Knight^{1,2,7,a}, M. Mallar
4 Chakravarty^{3,4,8,a*}

5
6 ¹ Campbell Family Mental Health Research Institute, Centre for Addiction and Mental Health, Toronto,
7 ON, Canada

8 ² Institute of Medical Science, University of Toronto, Toronto, ON, Canada

9 ³ Cerebral Imaging Centre, Douglas Mental Health University Institute, McGill University, Verdun, QC,
10 Canada

11 ⁴ Department of Biological and Biomedical Engineering, McGill University, Montreal, QC, Canada

12 ⁵ Schulich School of Medicine and Dentistry, Western University, London, ON, Canada

13 ⁶ Department of Neurology, Sunnybrook Health Sciences Centre, Toronto, ON, Canada

14 ⁷ Lancaster Medical School, Faculty of Health and Medicine, Lancaster University, Lancaster, UK

15 ⁸ Department of Psychiatry, McGill University, Montreal, QC, Canada

16 *** Corresponding authors at:**

17 Sejal Patel, Campbell Family Mental Health Research Institute, Centre for Addiction and Mental Health,
18 250 College Street, Toronto, ON, M5T 1R8, Canada

19 Email address: Sejal.Patel@camh.ca (S. Patel)

20 M. Mallar Chakravarty, Cerebral Imaging Centre, Douglas Mental Health University Institute, McGill
21 University, 6875 Boulevard LaSalle, Verdun, QC, H4H 1R3 Verdun, Canada

22 Email address: mallar@cobralab.ca (M.M. Chakravarty).

23 ^a M. Mallar Chakravarty and Jo Knight contributed equally as senior authors to this manuscript.

24 **ABSTRACT**

25 Twin study designs have been previously used to investigate the heritability of neuroanatomical
26 measures, such as regional cortical volumes. Volume can be fractionated into surface area and cortical
27 thickness, where both measures are considered to have independent genetic and environmental bases.
28 Region of interest (ROI) and vertex-wise approaches have been used to calculate heritability of cortical
29 thickness and surface area in twin studies. In our study, we estimate heritability using the Human
30 Connectome Project magnetic resonance imaging dataset composed of healthy young twin and non-twin
31 siblings (mean age of 29, sample size of 757). Both ROI and vertex-wise methods were used to
32 compare regional heritability of cortical thickness and surface area. Heritability estimates were
33 controlled for age, sex, and total ipsilateral surface area or mean cortical thickness. In both approaches,
34 heritability estimates of cortical thickness and surface area were lower when accounting for average
35 ipsilateral cortical thickness and total surface area respectively. When comparing both approaches at a
36 regional level, the vertex-wise approach showed higher surface area and lower cortical thickness
37 heritability estimates compared to the ROI approach. The calcarine fissure had the highest surface area
38 heritability estimate (ROI: 44%, vertex-wise: 50%) and posterior cingulate gyrus had the highest cortical
39 thickness heritability (ROI: 50%, vertex-wise 40%). We also observed that limitations in image
40 processing and variability in spatial averaging errors based on regional size may make obtaining true
41 estimates of cortical thickness and surface area challenging in smaller regions. It is important to identify
42 which approach is best suited to estimate heritability based on the research hypothesis and the size of the
43 regions being investigated.

44

45 **Keywords:** Heritability, Cortical thickness, Surface area, Extended twin design, Region of interest
46 approach, Vertex-wise approach

47 1. INTRODUCTION

48 Many twin studies have explored the variability of neuroanatomical measures (Baare et al., 2001; Eyler
49 et al., 2012; Panizzon et al., 2009; Pennington et al., 2000; Thompson et al., 2001a; Winkler et al.,
50 2010). In twin studies, three factors are typically used to explain the variation within a trait, namely:
51 genetics, shared and unique environment. Heritability is defined as the proportion of inherited genetic
52 variation observed within the trait (Jacquard, 1983). While some previous studies have investigated the
53 heritability of regional cortical volumes (Baare et al., 2001; Geschwind et al., 2002; Kremen et al., 2010;
54 Patel et al., 2017; Pennington et al., 2000; Thompson et al., 2014), it is critical to consider that volume
55 can be fractionated into surface area (SA) and cortical thickness components (CT), each of which is
56 suspected to have an independent genetic basis and relationship to environmental factors. At a cellular
57 level, local measures of cortical SA are thought to be defined by the number of neuronal columns per
58 unit area that result from the migration of neurons along radial glial cells during neurodevelopment
59 (Rakic, 1988, 2007). By contrast, CT measures represent the number of cells in a column across radial
60 glia during embryonic and fetal brain development (Rakic, 1988). However, in spite of their proximity,
61 the genetic correlation between SA and CT (the shared genetic variation between two traits), has been
62 reported to be near zero in twins (Panizzon et al., 2009) and family pedigree studies (Winkler et al.,
63 2010). CT and SA measures from both region of interest (ROI) and vertex-wise approaches have been
64 used in the investigation of the heritability on these measures of different brain structures (Eyler et al.,
65 2012; Ge et al., 2015; Panizzon et al., 2009; Rimol et al., 2010; Winkler et al., 2010). In the ROI
66 approach heritability is calculated on average CT and total SA of brain regions and vertex-wise
67 heritability estimates are based on CT and SA at each vertex across the brain. The effects of genetic
68 variation on measures across the brain can be continuous, making it difficult to map to restricted
69 boundaries found in the ROI approach. The vertex-wise approach can capture these patterns by creating
70 a continuous surface heritability brain map without being restricted to regional boundaries.

71
72 In our study, we compare regional heritability of CT and SA by using both ROI and vertex-wise
73 methods. Previous studies (Docherty et al., 2015; Eyler et al., 2012; Panizzon et al., 2009), have used the
74 Vietnam Era Twin Study of Aging data however, this consists only of elder male twin pairs (average age
75 of 55.8 years). We take advantage of the Human Connectome Project (HCP) having higher resolution
76 magnetic resonance imaging (MRI) data and a healthy young sample composed of not only males but
77 also female twins along with non-twin siblings. We further investigate the influence of total SA and
78 mean CT on both measures that we examine. In addition, we explore potential reasons for heritability
79 estimates to be underestimated in the ROI approach, an observation seen in the current and previous

80 studies (Eyer et al., 2012). The work presented in this manuscript can be used in the future for critical
81 examination of neuroimaging endophenotypes in imaging-genetics studies.

82

ACCEPTED MANUSCRIPT

83 2. METHODS

84 2.1. Human Connectome Project Dataset

85 Heritability analysis was performed using the Human Connectome Project (HCP) data. The aim of the
86 HCP is to investigate the connection between neuroanatomical structures with function and behavioural
87 traits of healthy adults (Van Essen et al., 2013). Investigators from Washington University St. Louis,
88 University of Minnesota, and Oxford University (the WU-Minn HCP consortium) lead the consortium
89 with an aim to recruit 1200 healthy twin and non-twin sibling adults (Van Essen et al., 2013). Data
90 collection started in 2013 and the data is publically available. The final dataset is designed to capture the
91 ethnic, racial, behavioural and economic demographic variability of the United States. Individuals with
92 high blood pressure and diabetes were excluded as are those with siblings who had neurodevelopmental,
93 neuropsychiatric, or neurological disorders. Premature twins (born before 34 weeks gestation) and non-
94 twins (born before 37 weeks gestation) were excluded. Individuals who were overweight or who were
95 smokers were included in the study. Individuals with a history of heavy drinking or use of a recreational
96 drug who have not experienced severe symptoms (e.g., individual not hospitalized for substance abuse
97 for two days or more) were included to be used for future psychiatric studies (Van Essen et al., 2013).
98 For more information on the inclusion and exclusion criteria, see supplemental Table S1 of Van Essen
99 DC et al., 2013.

100
101 Data used in this study is from the December 2015 release (900 subjects of which 875 had MRI). High-
102 resolution MRI was collected using a Siemens 3 Tesla (T) Skyra scanner (Van Essen et al., 2012). To
103 increase the maximum gradient strength, the scanner was modified with a Siemens SC72 gradient coil
104 from 40 mT/m to 100 mT/m (Van Essen et al., 2013; Van Essen et al., 2012). In our study, we used 3T,
105 high-resolution T1-weighted MRI (0.7mm isotropic voxel dimensions). The acquisition parameters
106 were: inversion time = 1000ms, echo time = 2.14ms, repetition time = 2400ms, acquisition time = 7min
107 40sec, flip angle = 8 degrees and field of view = 224mm x 224mm (Van Essen et al., 2012).

109 2.2. Image processing

110 For the work presented in this manuscript we obtained preprocessed T1-w data from the HCP. Detailed
111 information on the preprocessing steps can be found in the HCP S900 Release Reference Manual and
112 Glasser et al., (2014). Briefly, the preprocessing steps included: gradient distortion correction, co-
113 registration of T1-w runs and averaging of the runs, ACPC registration for distortion correction which
114 are done in native volume space. In addition, initial brain extraction, along with field map and bias field
115 correction and atlas registration was done (Glasser et al., 2014; Glasser et al., 2013). Then HCP images

116 were further processed in our lab using minc-bpipe-library ([https://github.com/CobraLab/minc-bpipe-](https://github.com/CobraLab/minc-bpipe-library.git)
117 [library.git](https://github.com/CobraLab/minc-bpipe-library.git)). N4 correction was applied to correct for intensity non-uniformity across the image before
118 analysis of CT and SA. The N4 correction helps improve images to pass quality control, during the
119 downstream analysis.

120
121 After processing the images using the minc-bpipe library, CIVET 1.1.12 pipeline (Ad-Dab'bagh et al.,
122 2006; Collins et al., 1994; Lerch and Evans, 2005; MacDonald et al., 2000) was used to measure CT and
123 SA of T1-weighted MRI scans. In CIVET, each subject's surfaces are registered to a study specific
124 average derived from the population under study. This iterative approach was used to find the optimal
125 vertex as described by Lyttelton et al., (2007). T1 weighted images of $0.7 \times 0.7 \times 0.7 \text{mm}^3$ isotropic voxel
126 dimension were used in the CIVET pipeline with the following parameters: N3 correction of non-
127 uniformities was set to a distance of 50, affine 12-parameter transformation to stereotaxic space was
128 used and the cortical surfaces were resampled to obtain vertex-based areas. CT and SA were output
129 separately for the left and right hemisphere. The Anatomical Automatic Labeling (AAL) atlas is defined
130 in the vertex-wise space, a label number for each vertex corresponded to a region within the atlas.
131 Briefly, first the images were registered linearly to standard stereotaxic space as defined by the MNI
132 ICBM 152 model (Collins et al., 1994). Then for each subject, each voxel is classified as white matter
133 (WM), gray matter (GM) or cerebrospinal fluid (CSF). A deformable ellipsoid polygonal surface mesh
134 model is used to fit the WM and GM interface in order to generate the WM surface. The GM surface is
135 generated by expanding the WM surface to the GM/pial interface using the Laplacian approach (Kim et
136 al., 2005). Each of the final meshes has 40,962 vertices within each hemisphere and CT is estimated in
137 millimeters (mm), between WM surface and GM surface at each vertex (Lerch and Evans, 2005). A
138 surface based smoothing kernel of 20mm full-width at half maximum (FWHM) was applied to CT data.
139 SA of each vertex is calculated at the middle cortical surface (the geometric center between the inner
140 and outer cortical surface). SA at each vertex is estimated as the average area of the 6 triangles
141 connected to that specific vertex (Lyttelton et al., 2007). For the SA data, a surface based smoothing
142 kernel of 40mm FWHM was applied. In the CIVET analysis the AAL atlas is used to calculate the
143 average CT and SA for defined regions (Tzourio-Mazoyer et al., 2002). These values were used in the
144 ROI approach to calculate heritability estimates. In total there are 39 regions for each hemisphere where
145 each vertex of the 40,962 vertices is allocated within each AAL parcellations.

146

147 On all resultant outputs from CIVET, we performed intense manual quality control of the images to
148 examine possible confounds due to blood vessels or dura that may be captured by the algorithm. A total

149 of 875 subjects from the HCP data were processed using CIVET to extract CT and SA at each vertex.
150 From the 875 subjects 840 passed manual quality control which was further reduced to 757 subjects
151 after removal of individuals with no siblings within the families.

152

153 **2.3. Heritability estimates for vertex-wise and ROI approach**

154 *Vertex-wise approach:* Heritability was estimated at each vertex on the cortex for both SA and CT
155 measures. Average and standard deviations of heritability were estimated in the vertex-wise approach
156 for all vertices labelled within a region of the AAL atlas.

157 *ROI approach:* Heritability and 95% confidence intervals were estimated based on mean CT and total
158 SA of each region defined by the AAL atlas. In OpenMx, confidence intervals was calculated from the
159 maximum likelihood estimates on the parameters A , C , and E (Neale and Miller, 1997).

160

161 **2.4. Verification of distributions**

162 We examined the normality of the average CT and total SA measurement for each region within the
163 AAL atlas before estimating heritability within the ROI approach. Shapiro-Wilk normality test was
164 applied for all the 39 regions in both the right and left hemispheres defined by the AAL atlas.

165

166 **2.5. Heritability calculations**

167 Broad-sense heritability of CT and SA in both the vertex-wise and ROI approach was estimated using
168 OpenMx version 2.6.9 (Neale et al., 2016) R package. Heritability is defined as the ratio of variance
169 from a phenotypic measurement (as defined by a numerator of genetic variation $[A]$ and denominator of
170 the total observed variation due to genetics $[A]$, shared environment $[C]$ and unique environment $[E]$). In
171 our analyses we defined shared environment $[C]$ as being identical within a family ($C=1$ for all siblings
172 within a family). We set $A=1$ for MZ twin pairs under the assumption of identical genetic makeup and
173 $A=0.5$ for DZ twins under the assumption that non-twin siblings share ~50% of all genetics (Jacquard,
174 1983; Plomin et al., 1976). Since MZ twins have identical genetic makeup, it is worth considering that
175 this is likely to lead to greater similarity in cortical morphology, in terms of sulci and gyri location. This
176 can be a possible confounding factor resulting into higher heritability estimates in SA. Therefore, before
177 drawing conclusions from heritability estimates we need to keep in mind that there are factors such as
178 similar morphology which are not accounted for in the calculations and may bias the results.

179

180 Full ACE univariate models were used for both vertex-wise and ROI approaches. The final sample size
181 used for heritability calculation was 757 individuals including: 168 MZ twins, 158 DZ twins and 431
182 non-twin siblings (total of 282 families, 37 families had only twin pairs, 126 families had twin pairs with
183 non-twin siblings and 119 families consisted of non-twin siblings only). **To address the concern of**
184 **discordant sex sibling on heritability estimates, a sensitivity analysis was performed on same sex**
185 **siblings calculating heritability estimates. The number of same sex DZ twin pairs were 78 out of**
186 **79. In our sample the majority of non-twin sibling families were sex discordant. Therefore**
187 **isolating non-twin sibling pairs of the same sex reduced the sample size greatly. See**
188 **Supplementary section: Sensitivity Analysis (Same sex sample, see Inline Supplementary Table**
189 **S8) for results on same sex sibling sample. To account for the sex differences, a direct way of**
190 **minimizing the impact of biological sex is to adjust or remove sex on SA and CT for each**
191 **individual via a general linear model.** As a result, the heritability estimates are based on the newly
192 adjusted measures within our model. Furthermore, heritability was estimated in two different analysis in
193 order to examine the influence of total brain size: 1) adjusting for sex and age (henceforth referred to as
194 'partially adjusted') and 2) adjusting for sex, age and ipsilateral total brain SA or ipsilateral average
195 brain CT, known as 'completely adjusted'.

196

197 **2.6. Investigation of near-zero heritability:**

198 During our analyses we observed that some regions had heritability estimates of zero or near zero at the
199 vertex-level and in the ROI approach. To further investigate these results, we explored the twin
200 correlation of CT and SA within the vertex-wise and ROI approach for both the MZ and DZ twin pairs.
201 To adjust for vertex-level heritability measures, vertices with <1% heritability were removed from the
202 estimation of the averages.

3. RESULTS

3.1. Human Connectome Project demographics

After quality control of images processed through CIVET and removal of families with only one individual, the final sample size used for heritability analysis was 757 subjects, which included 424 women and 333 men with an age range of 22-37 years old and with an average age of 28.90 (3.62± SD) years old. The Edinburgh inventory was used to measure handedness (Oldfield, 1971), the average handedness for our sample was 65.33(45.14±SD). The scale for handedness ranges from -100 (left-hand dominant) to 100 (right-hand dominant). Fluid intelligence was measured using the Raven's Progressive Matrices test, the number of correct responses were out of 24 questions with an overall average of 16.55(4.85± SD). Demographic information is summarized in Table 1.

TABLE 1. Demographic breakdown of monozygotic twins (MZ), dizygotic twins (DZ) and non-twin siblings from the subset data of the HCP, including averages and standard deviation (± SD)

	N	Average Age (year ± SD)	Age Range	Sex Female: Male	Average handedness (± SD)	Average fluid intelligence (± SD)
MZ	168	29.83(3.36)	22-36	120:48	68.75(46.13)	16.21 (4.66)
DZ	158	28.98(3.32)	22-35	91:134	64.62(42.39)	17.02(4.78)
Non-twin siblings	431	28.51(3.75)	22-37	213:218	64.26(45.75)	16.51(4.94)
Total	757	28.90(3.62)	22-37	424:333	65.33(45.14)	16.55(4.85)

3.2. Imaging processing: Average CT and total brain SA heritability estimates

The average mean brain CT was 3.33mm ±0.11 SD and 3.32mm ±0.11 SD, left and right hemisphere respectively. The average total brain SA was 94065.30mm² ±8213.00 SD and 94502.79mm² ±8306.58 SD, left and right hemisphere respectively. Table 2 includes the average mean brain CT and total brain SA along with standard deviation for MZ, DZ and non-twin siblings. Lower SA is seen in MZ twins compared to DZ twins and non-twin siblings; potentially due to higher ratio of females in MZ groups compared to the other two groups. Overall, after adjusting for sex and age the heritability of mean CT was 46% (left) and 67% (right). Furthermore the heritability of total brain SA was 75% (left) and 73% (right).

TABLE 2. Average left and right mean brain cortical thickness (CT) and total brain surface area (SA) and standard deviation (±SD) in monozygotic twins (MZ), dizygotic twins (DZ) and non-twin siblings.

Sample	N	Average mean left CT (mm ± SD)	Average mean right CT (mm ± SD)	Average total left SA (mm ² ± SD)	Average total right SA (mm ² ± SD)
MZ	168	3.32 (±0.11)	3.32(±0.10)	91581.25 (±7284.53)	92033.74 (±7480.45)

DZ	158	3.35 (± 0.10)	3.34(± 0.10)	94013.8 (± 84013.8)	94487.53 (± 8530.80)
Non-twin siblings	431	3.33 (± 0.12)	3.33 (± 0.12)	95052.43 (± 8293.25)	95470.80 (± 8347.81)
Total	757	3.33 (± 0.11)	3.32 (± 0.11)	94065.30 (± 8213.00)	94502.79 (± 8306.58)

228

229 **3.3. Verification of distributions**

230 In the ROI approach, a Shapiro-Wilk normality distribution test was performed on regions defined using
 231 the AAL atlas revealed that some regions for both CT and SA (partially and completely adjusted) were
 232 not normally distributed. This was observed at the level of SA measures of smaller regions such as the
 233 Heschl Gyrus. P values for each region are shown in the supplementary section, see Inline
 234 Supplementary Table S1. As many distributions were skewed we attempted to transform the data using a
 235 LOG transformation, however heritability estimates before and after transformation were similar.
 236 Therefore, we used non-transformed data for heritability calculations. In literature it has been shown that
 237 SEM is robust when dealing with violation of normality within a dataset (Bollen, 1989; Diamantopoulos
 238 et al., 2000). In addition Reinartz et al (2009) observed no major differences using maximum likelihood
 239 estimator on different kurtosis and skewness levels of samples (Reinartz et al., 2009).

240

241 **3.4. Vertex-wise approach: High heritability estimates in SA compared to CT**

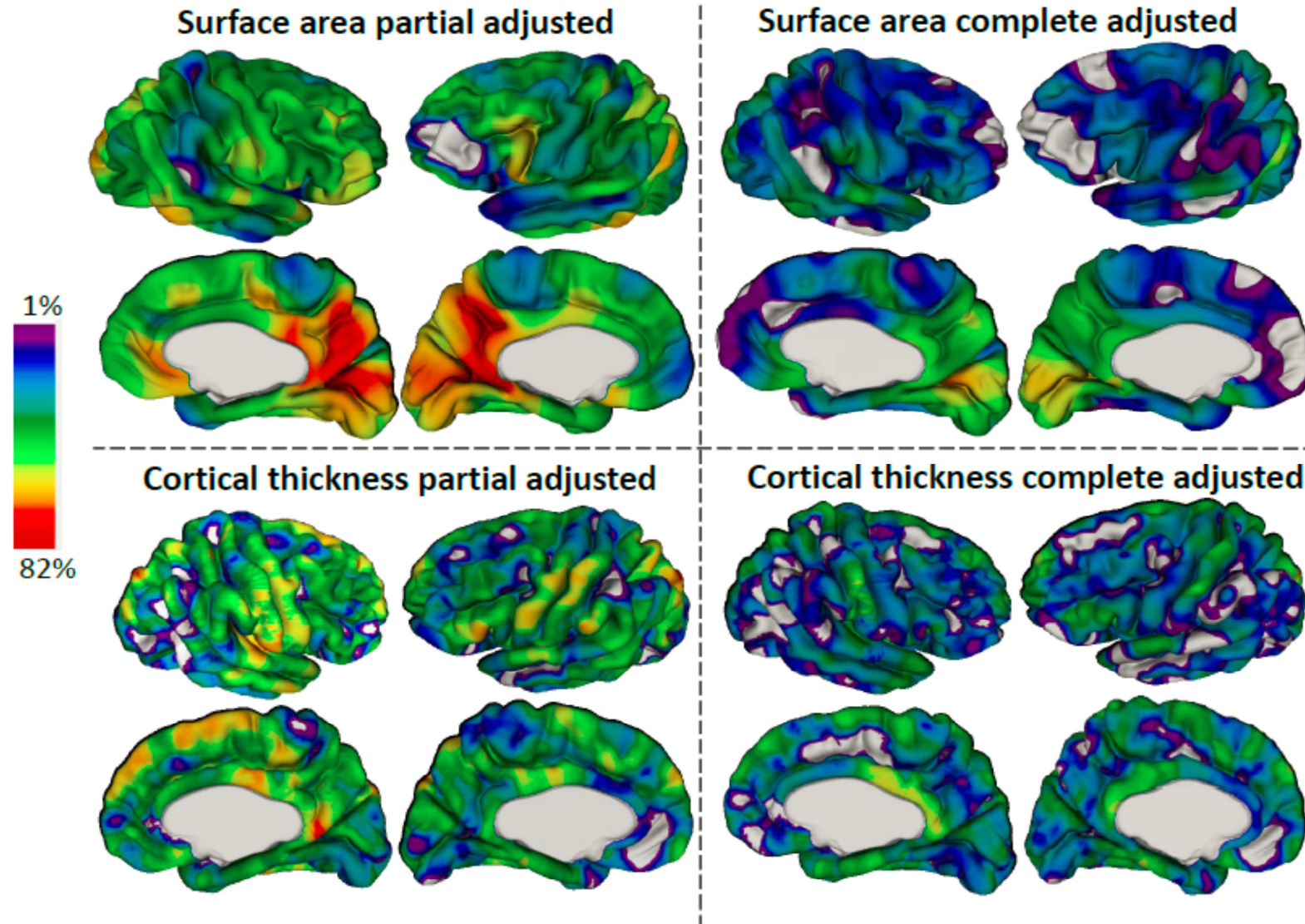
242 Overall, vertex-wise average heritability estimates were higher in SA compared to CT for both partially
 243 and completely adjusted values for most of the brain regions. Specifically, high heritability estimates
 244 were observed within regions of the occipital lobe (Table 3; see Inline Supplementary Figure S1a-b).
 245 See Inline Supplementary Table S2a for vertex-wise average heritability estimates along with standard
 246 deviations.

247

248 In the vertex-wise approach there were a portion of vertices that had zero or near zero heritability
 249 estimates, vertices with heritability less than 1% were removed (we later show the zeros are likely to be
 250 due to the estimation errors, see section 4). For partially adjusted CT and SA measures, the portion of
 251 vertices removed was 3% and 1% respectively. For completely adjusted measures, 8% of CT and 7% of
 252 SA vertices were removed. See Inline Supplementary Table S2b for the total number of vertices within
 253 the region used to calculate average heritability estimates before and after adjustments. Figure 1a shows
 254 a surface-map of heritability estimates of partially and completely adjusted CT and SA mapped at each
 255 vertex of the brain (40,962 vertices in each hemisphere). In partial and complete adjustments for CT,

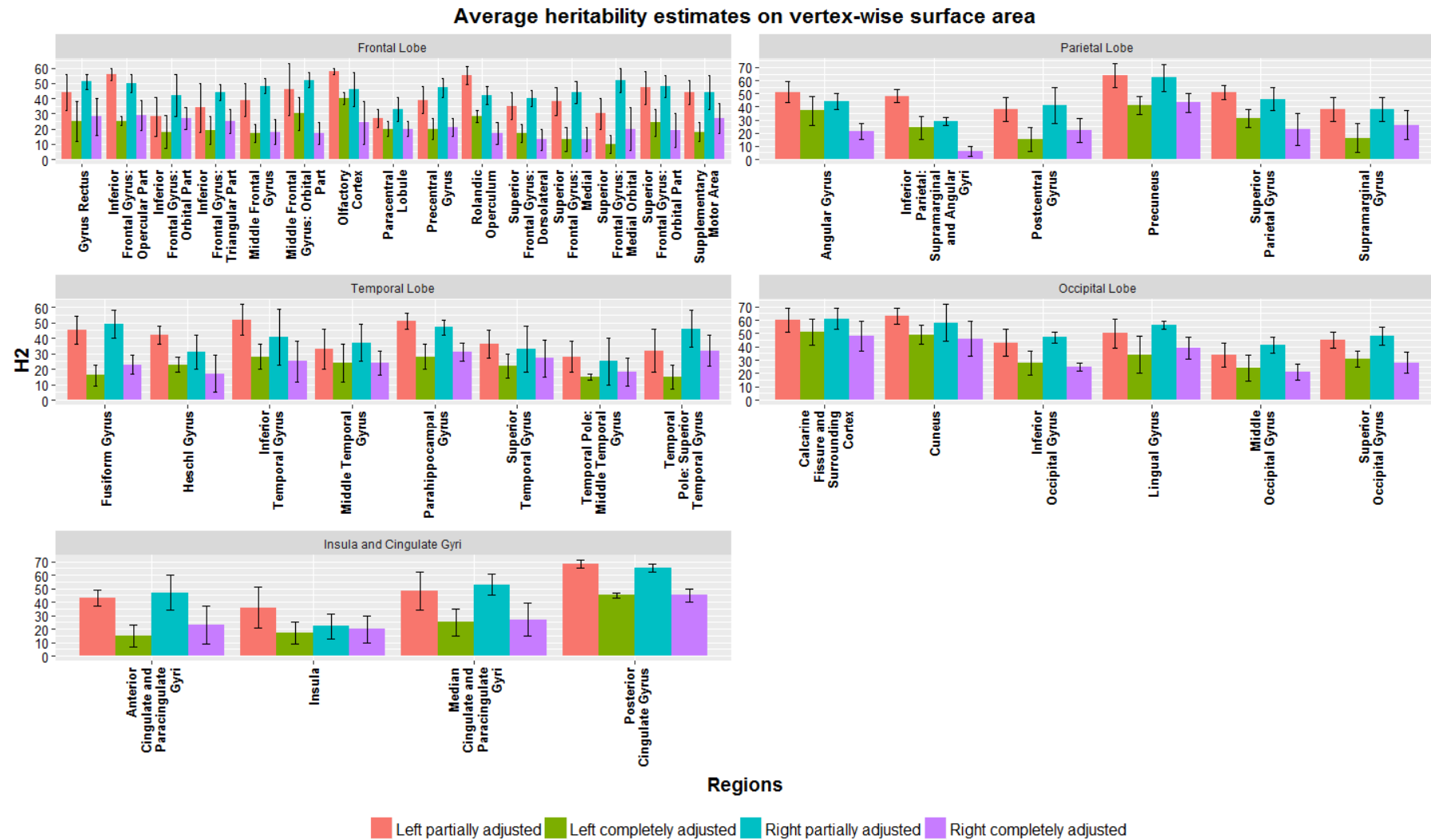
256 heritability estimates of less than 1% (grey colour) are scattered throughout the brain whereas for SA,
257 they were predominantly found in the frontal lobe regions, and in parts of the superior temporal gyrus
258 (Figure 1a). See Inline Supplementary Figure S1c-d for complete analysis of brain maps on common and
259 shared environment. Figure 1a showed a lower heritability estimates after complete adjustment for both
260 CT and SA compared to partially adjusted measures. Average heritability estimates for partially adjusted
261 SA ranged from 22% (right insula) to 68% (left posterior cingulate gyrus) and were lower in the
262 completely adjusted SA model (Table 3, Figure 1b), ranging from 6% (right inferior parietal) to 51%
263 (left calcarine fissure and surrounding cortex). For partially adjusted CT the average heritability
264 estimates ranged from 17% (left anterior cingulate and paracingulate gyri) to 54% (right rolandic
265 operculum) and decreased in completely adjusted CT from 12% (right inferior parietal) to 42% (right
266 posterior cingulate gyrus) (Table 3, Figure 1c).

267 **Figure 1a.** Vertex-wise heritability map of partially adjusted (sex and age) and completely adjusted (sex, age, ipsilateral average brain
268 cortical thickness or ipsilateral total brain surface area) cortical thickness and surface area. Regions in which vertices with heritability
269 estimates of less than 1% are coloured grey.



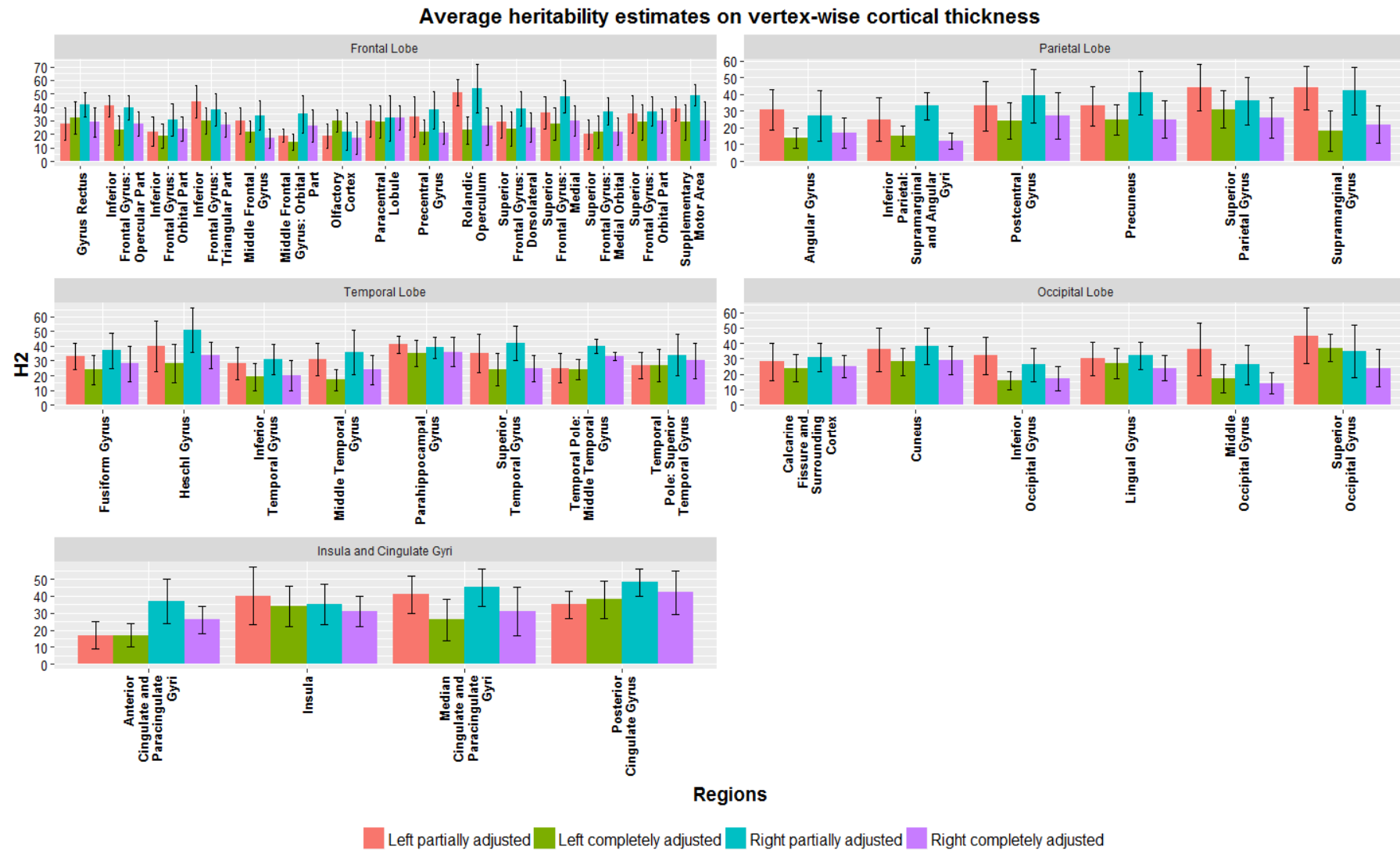
270

271 **Figure 1b. Average heritability estimates (H2) on vertex-wise surface area (SA) for partially adjusted (controlled for sex and age) and**
 272 **completely adjusted value (controlled for sex, age, ipsilateral total brain surface area). Average heritability estimates are calculated in**
 273 **left and right regions of the AAL atlas. The error bars for the vertex-wise approach represent the standard deviation from the**
 274 **averaged heritability estimates.**



275

276 **Figure 1c. Average heritability estimates (H2) on vertex-wise cortical thickness (CT) for partially adjusted (controlled for sex and age)**
 277 **and completely adjusted value (controlled for sex, age, average brain cortical thickness). Average heritability estimates are calculated**
 278 **in left and right regions of the AAL atlas. The error bars for the vertex-wise approach represent the standard deviation from the**
 279 **averaged heritability estimates.**



280

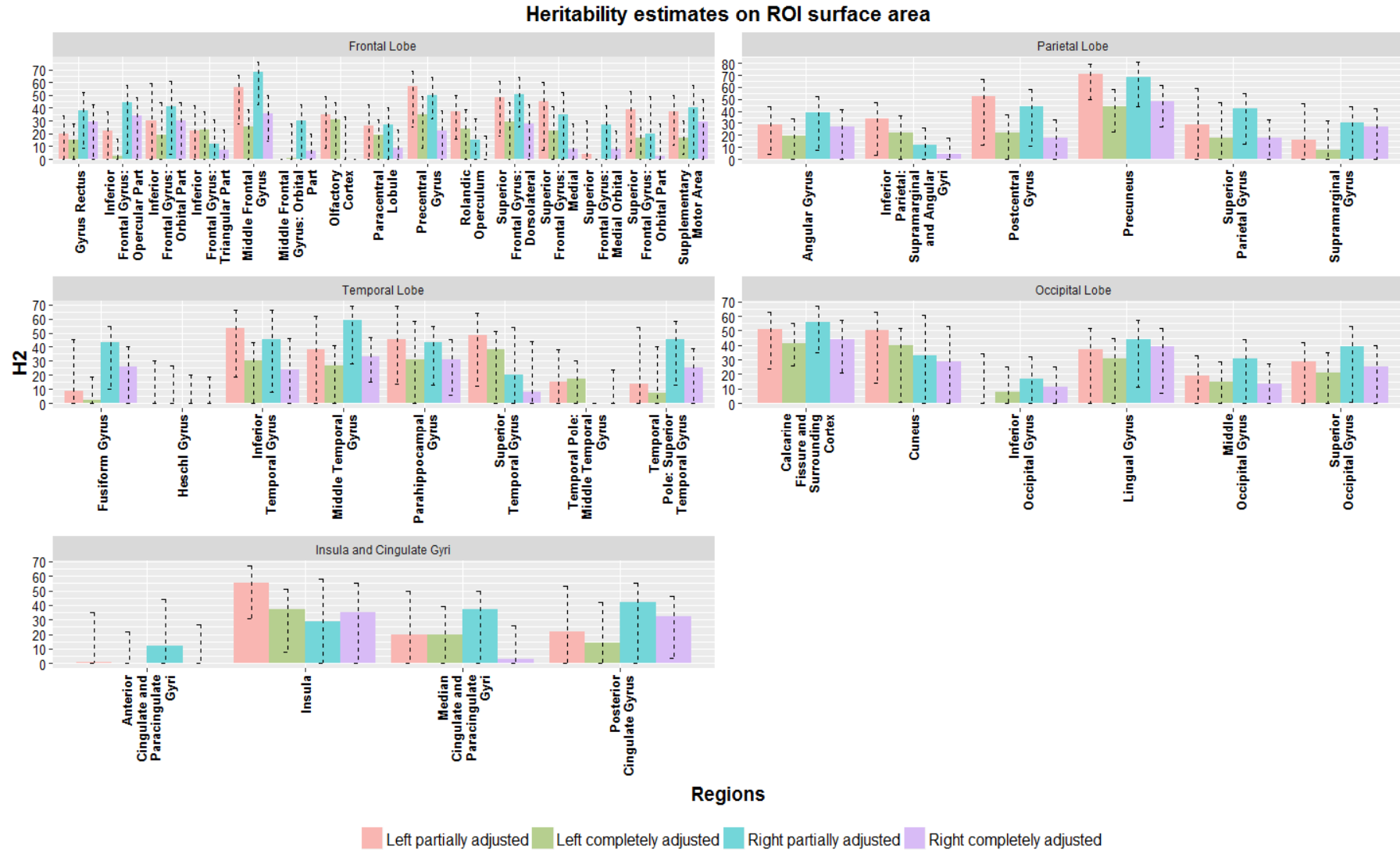
281 3.5. ROI approach: High heritability estimates in CT compared to SA

282 Overall, in the ROI approach, most regions had higher heritability estimates of CT than SA in both
283 partially and completely adjusted values (Table 3; see Inline Supplementary Figure S2a-b). See Inline
284 Supplementary Table S3 for ROI heritability estimates with confidence intervals.

285

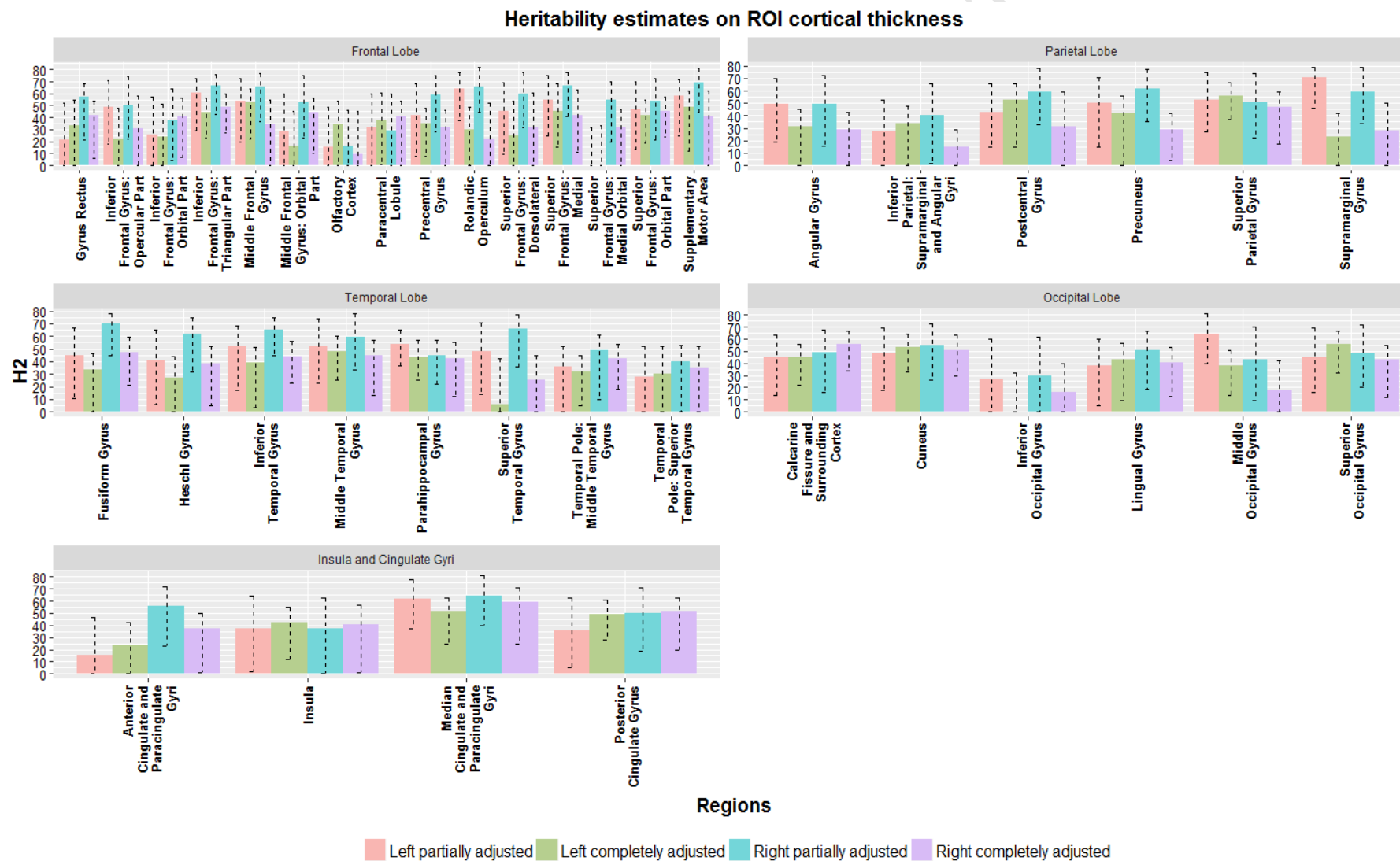
286 In partially adjusted SA the heritability ranged from 4% (left superior frontal gyrus: medial orbital) to
287 71% (left precuneus) and after complete adjustment, the heritability estimates were lower in the range
288 from 2% (left middle frontal gyrus orbital part and right superior frontal gyrus orbital part) to 48% (right
289 precuneus), Table 3 and Figure 2a. Furthermore, the heritability estimates of partially adjusted CT
290 ranged from 16% (right olfactory cortex) to 71% (left supramarginal gyrus) and decreased moderately
291 after complete adjustment from 6% (left superior temporal gyrus) to 59% (median cingulate and
292 paracingulate gyri), Table 3 and Figure 2b.

293 **Figure 2a. ROI approach of heritability estimates (H2) on total surface area (SA) for partially adjusted (controlled for sex, age,) and**
 294 **completely adjusted value (controlled for sex, age, ipsilateral total brain surface area) within left and right regions defined using the**
 295 **AAL atlas. The dashed error bars in the ROI approach represent 95% confidence intervals from maximum likelihood estimates on the**
 296 **parameters A (genetics).**



297

298 **Figure 2b. ROI approach of heritability estimates (H2) on mean cortical thickness (CT) for partially adjusted (controlled for sex, age,)**
 299 **and completely adjusted value (controlled for sex, age and ipsilateral average brain cortical thickness) within left and right regions**
 300 **defined using the AAL atlas. The dashed error bars in the ROI approach represent 95% confidence intervals from maximum**
 301 **likelihood estimates on the parameters A (genetics).**



302

303 3.6. ROI and vertex-wise approach: Heritability estimates of zero

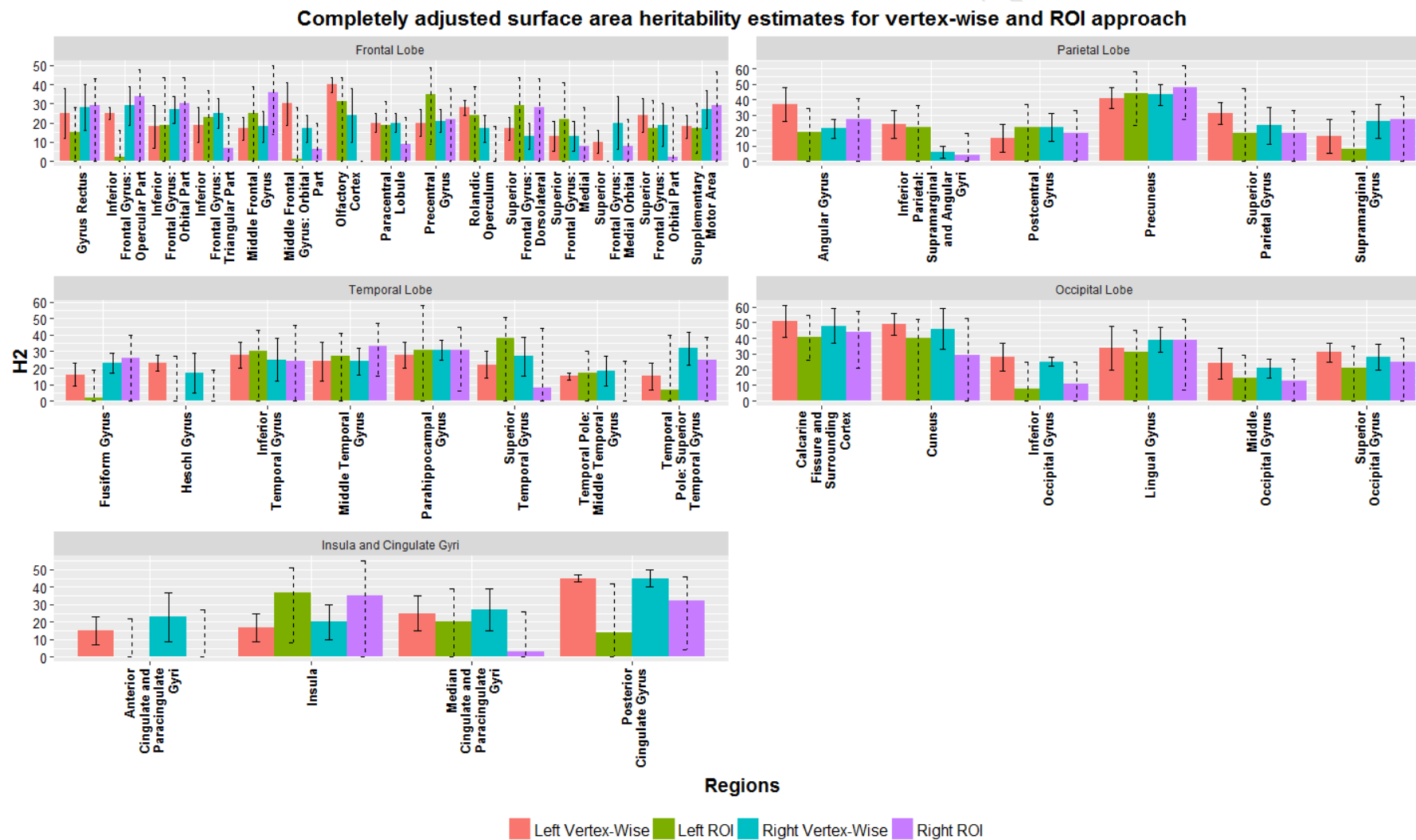
304 In the ROI approach, we noticed that some regions either in the left/right partially or completely
305 adjusted models had heritability estimates near zero for SA and CT (Table 2). Similarly, this was also
306 observed in the vertex-wise approach, a subset of number of vertices had heritability estimates of zero.
307 In both approaches, the MZ twin correlation compared to DZ twins for both SA and CT was lower in a
308 subset of vertices and in smaller regions. See Inline Supplementary Table S4 for exploratory analysis of
309 MZ and DZ twin correlation on a subset of vertices and Table S5 for smaller regions in the ROI
310 approach with heritability estimates of zero. We selected 5 large regions from the AAL atlas that had
311 heritability estimates not near zero (supplementary table S6) using the ROI approach, as expected MZ
312 twin correlation was larger or near DZ twin correlation, unlike the small regions.

313

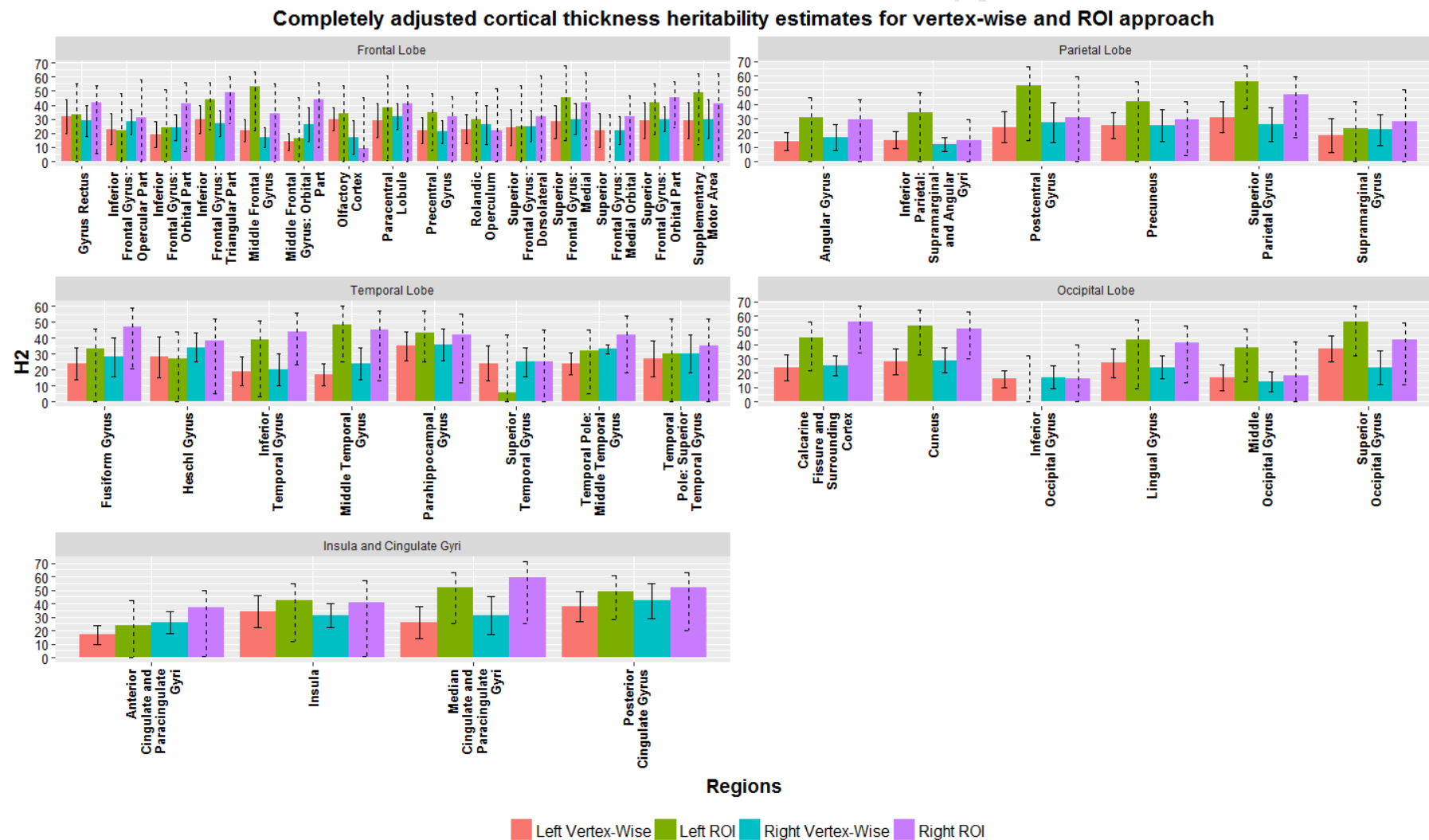
314 3.7. Higher SA and lower CT heritability estimate in the vertex-wise compared to ROI approach

315 Overall, the adjusted ROI heritability estimates were lower compared to vertex-wise average heritability
316 estimates of SA. However, in contrast, the ROI approach had higher heritability estimates of CT than the
317 vertex-wise approach (Table 2, Figure 3a-b). To show this trend we compared completely adjusted
318 heritability estimates of CT (Figure 3c) and SA (Figure 3d) between both approaches of 5 selected
319 regions. Each region was selected within each lobe of the brain in order to best represent the whole
320 brain. The regions selected were the left and right calcarine fissure, temporal pole (superior temporal
321 gyrus), superior parietal gyrus, paracentral lobule and posterior cingulate gyrus. In the vertex-wise
322 approach the standard error represents the standard deviation from the averaged heritability estimates
323 and in the ROI approach the error bars are 95% confidence intervals (Figure 3c-d).

324 **Figure 3a. Completely adjusted left/right surface area (SA) heritability estimate H^2 for vertex-wise and ROI approach. Completely**
 325 **adjusted values are controlled for sex, age and ipsilateral total brain surface area. Solid error bars for the vertex-wise approach**
 326 **represent the standard deviation from the averaged heritability estimates. Dashed error bars in the ROI approach represent 95%**
 327 **confidence intervals.**

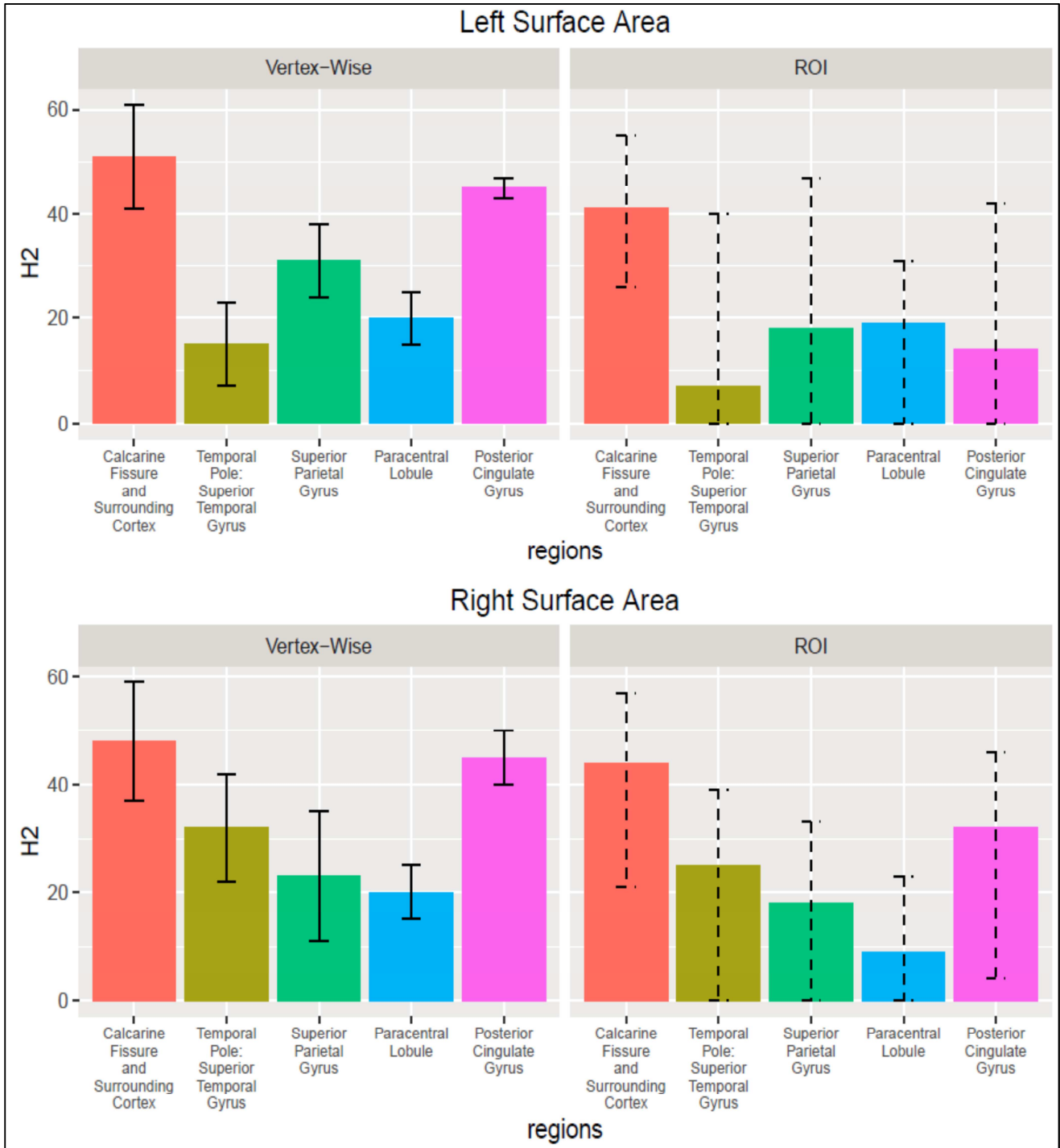


329 **Figure 3b. Completely adjusted left/right cortical thickness (CT) heritability estimate H^2 for vertex-wise and ROI approach.**
 330 **Completely adjusted values are control for sex, age and ipsilateral average brain cortical thickness. Solid error bars for the vertex-wise**
 331 **approach represent the standard deviation from the averaged heritability estimates. Dashed error bars in the ROI approach represent**
 332 **95% confidence intervals.**



333

334 **Figure 3c. Completely adjusted left/right surface area heritability estimate (H^2) for vertex-wise**
 335 **and ROI approach in 5 regions. Completely adjusted values are control for sex, age and ipsilateral**
 336 **total brain surface area. Solid error bars for the vertex-wise approach represent the standard**
 337 **deviation from the averaged heritability estimates. Dashed error bars in the ROI approach**
 338 **represent 95% confidence intervals.**

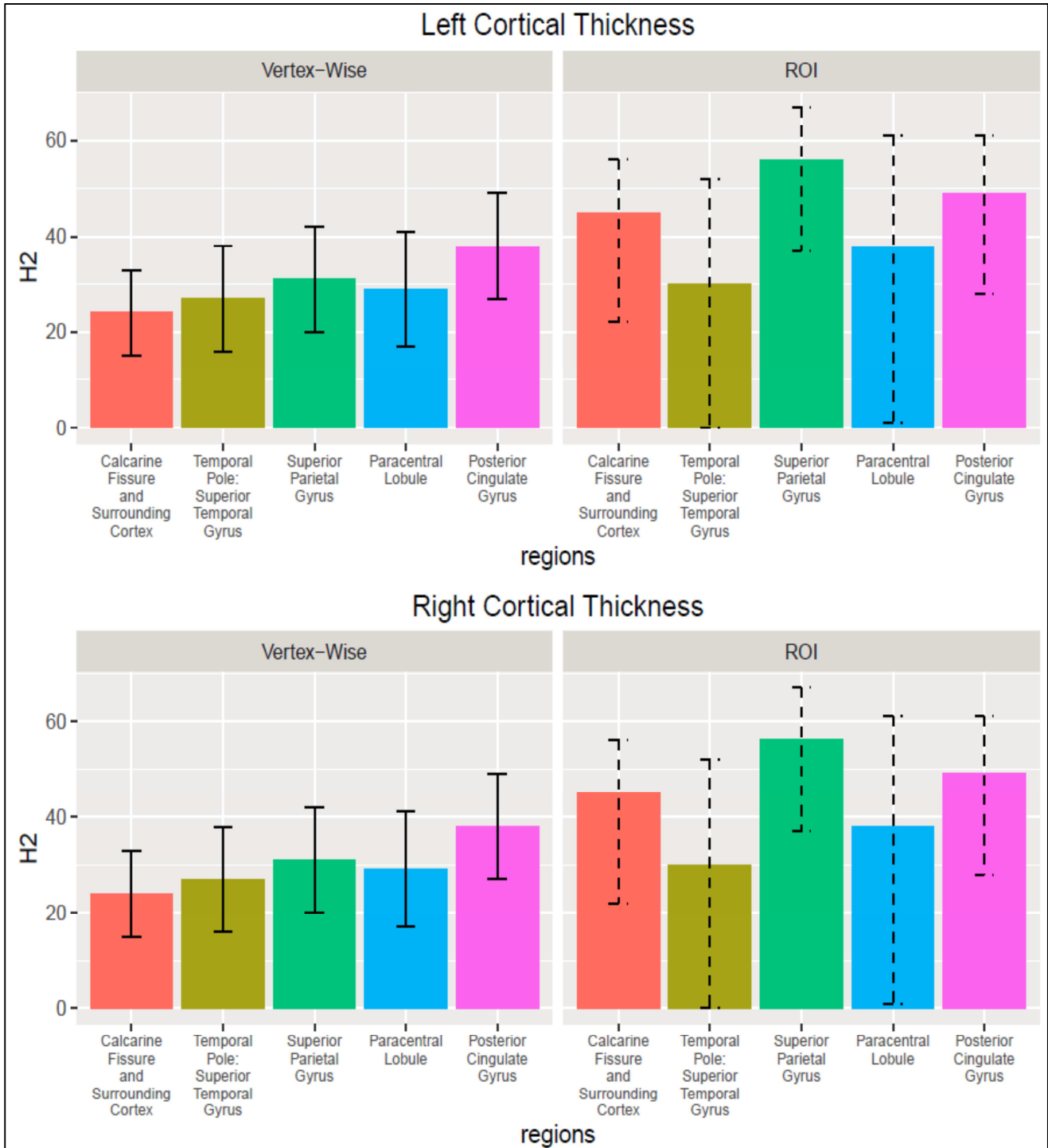


339

340

341

342 **Figure 3d. Completely adjusted left/right cortical thickness heritability estimate (H^2) for vertex-**
 343 **wise and ROI approach in 5 regions. Completely adjusted values are control for sex, age and**
 344 **ipsilateral average brain cortical thickness. Solid error bars for the vertex-wise approach**
 345 **represent the standard deviation from the averaged heritability estimates. Dashed error bars in**
 346 **the ROI approach represent 95% confidence intervals.**



347
348

349 **4. DISCUSSION**

350 In this study we investigated heritability estimates of CT and SA using both vertex-wise and ROI
351 approaches. Heritability estimates for both CT and SA were lower when accounting for ipsilateral
352 average brain CT and total brain SA, respectively. These findings suggest that there are regional
353 differences in heritability estimates after the influence of global measures are removed. This replicates
354 similar findings in previous studies (Eyler et al., 2012; Panizzon et al., 2009; Winkler et al., 2010). To
355 the best of our knowledge, there have been no studies of CT and SA heritability completed to date in a
356 young healthy population using a large dataset such as the HCP. The Vietnam Era Twin Study of Aging
357 data is a common dataset used in heritability studies, however it only contains elder male twins (age
358 range of 51 to 59 years). Males have large total brain volume compared to females (Kretschmann et al.,
359 1979; Swaab and Hofman, 1984), and since volume is the product of SA and CT, it is important to
360 examine heritability of a sample that better represents the general population including females.
361 Furthermore, along with male and female twins in our model, we also included non-twin siblings.
362 Adding non-twin siblings into the model increases statistical power to identify heritability (Posthuma
363 and Boomsma, 2000). Therefore the HCP which includes a young healthy population of males and
364 female (age range of 22-37) is a better representation of the general population to be used in heritability
365 analysis.

366
367 Overall, SA was observed to have higher heritability estimates than CT at a global and regional level.
368 This observation has also been seen in previous studies (Panizzon *et al.*, 2009, Winkler *et al.*, 2010),
369 suggesting that the genetic mechanisms underlying SA and CT measures differ. The study by Dochert et
370 al. (2015) demonstrated a slightly higher heritability of regional SA compared to CT after adjusting for
371 global SA and CT measures. This led to the interpretation that environmental factors may have a greater
372 influence on CT than SA. Similar to our findings, Eyler et al., 2012 showed high heritability estimates
373 near the parietal lobe. In our data, the precuneus and Calcarine Fissure were observed to have highly
374 heritable SA and CT measures. In contrast, we observed low heritability estimates in the precentral and
375 postcentral gyrus for both CT and SA compare to regions within the occipital lobe. Therefore, we
376 suggest that the architecture of the precentral and postcentral gyrus may be influenced by factors such as
377 sensory experience. In a heritability study using data from both pediatric and young adult twins, Lenroot
378 et al. (2008) observed lower heritability estimates in adults compared to young children within the
379 primary motor cortex (precentral gyrus) and somatosensory cortex (postcentral gyrus) (Lenroot and
380 Giedd, 2008). These regions play a role in daily sensory experiences and motor activities from
381 environmental cues (Thompson et al., 2001b), suggesting that the accumulation of environmental

382 exposures may decrease the influence of genetics. Furthermore, from an evolutionary perspective, the
383 primary somatosensory cortex in humans underwent more recent evolution, as of the need for finer
384 motor skills has increased (i.e., we have hands that have larger representation within brain than simple
385 paws do in lower order animals). Therefore, heritability may be lower in these regions due to the lack of
386 functional conservation within the region based on the adapted nature of brain function between species.
387 Regions that undergo somewhat more minimal evolutionary adaptation (such as primary occipital
388 region, which plays a role in basic function) may be prone to being more highly conserved across
389 species, therefore maintaining a more pronounced heritability (Kaas, 2008). It is important to consider
390 our findings of heritability in the context of evolution, brain development, and their relationship with
391 respect to cortical connectivity. The radial unit hypothesis has been used in literature to explain the
392 development of CT and SA at a cellular level (Rakic, 1988, 2009). SA has been altered dramatically
393 between humans and other primates compared to CT. The dramatic expansion of the cortical sheet
394 consistently observed in higher-order species (particularly in humans), has typically been associated
395 with the need to “fit” more of the cortical grey matter into a confined space defined by the skull.
396 Increased in CT does not necessarily reflect increases in long range connectivity. The radial glial units
397 that promote migration of neural progenitors and other cell types to the cortex eventually differentiate
398 into axons; therefore connectivity throughout the brain occurs at the same time that we begin to observe
399 expansion of the cortical sheet during development. Moreover, CT differences are likely to reflect
400 alteration in local architecture (at the level of cortical columns) as defined by local changes in synaptic
401 connectivity, changes in composition of glial cells, changes in neuronal number and size, and potentially
402 even cortical myelination (Barry et al., 2014; Noctor et al., 2001; Rakic, 1988, 2009; Steindler, 1993).
403 Long range white matter connections are unlikely to be impacted in this regard. Furthermore, the
404 discovery of intermediate progenitor cells (IPC) which develop into neurons has modified the radial unit
405 hypothesis (Noctor et al., 2004; Pontious et al., 2008). IPCs play a role in the modulation of SA
406 expansion at a regional level which defines the cortical cytoarchitecture (Pontious et al., 2008). If IPCs
407 are regionally specific this may support the increase in SA of the prefrontal region within humans which
408 plays a role in higher function compared to other primates. Reflecting back to our findings, a weak trend
409 is seen where CT heritability estimates were higher than SA in certain areas, such as the prefrontal
410 regions. The genetic etiology and evolution of CT and SA is complex and difficult to untangle its
411 influence on heritability estimates. Before drawing conclusions on regional heritability between CT and
412 SA of the brain, one needs to keep in mind many factors that influence the estimates such as function,
413 evolution between species and the genetic etiology of these measure.

414

415 The heritability estimates for SA after adjusting for ipsilateral total brain SA in the vertex-wise approach
416 were higher compared to the ROI approach when comparing corresponding regions. In contrast,
417 heritability estimates derived from the vertex-wise approach after adjusting for ipsilateral average brain
418 CT was lower in most regions compared to the ROI approach. When taking regional averages of
419 neuroanatomical measures, there is greater variability associated with taking an average of smaller
420 regions containing less vertices compared to larger regions in the ROI approach (Eyler et al., 2012).
421 Errors associated with spatial averaging may violate the assumption that MZ phenotypic twin correlation
422 should be equal to or greater than DZ twins for a given trait. This assumption within the model is not
423 met within smaller regions causing the model to fail resulting in heritability estimates of zero within
424 both approaches. Specifically, in the ROI approach we observed more instances of underestimated
425 heritability in smaller regions for SA compared to CT (such as Heschl gyrus, anterior cingulate and
426 paracingulate gyri). This can be due to the limitation in defining boundaries of smaller regions.
427 Heritability estimates in some regions are lower than expected, such as the orbitofrontal regions
428 compared to the precuneus region. The orbitofrontal regions within the AAL atlas is divided into 4 parts,
429 each part having a low number of vertices ranging from 350 vertices in the right middle frontal gyrus to
430 973 vertices in the right inferior frontal gyrus. Heritability estimates within these regions were low,
431 especially seen in the left middle frontal gyrus: orbital part having an estimate of 1% within the ROI
432 approach. In the precuneus region, the number of vertices are far more, around 2268, and there is an
433 associated high heritability estimates. Defining neuroanatomical measures of larger regions has less
434 variability across the sample, suggesting more reliable heritability scores. In addition, large variance
435 within the 95% confidence intervals was observed within smaller regions compared to larger regions in
436 the ROI approach. For example, the temporal pole is a smaller region compared to the superior parietal
437 gyrus which had wider 95% confidence interval variance that included 0% heritability estimate within
438 the interval for both CT and SA measures. The temporal pole is composed of 563 and 628 vertices (left
439 and right hemisphere respectively), however the superior parietal gyrus has greater number of vertices
440 (1336 and 1448, left and right hemisphere respectively). Therefore, confidence intervals that include 0
441 are disproportionately observed in regions that are smaller (based on number of vertices) compared to
442 larger regions, resulting in unreliable heritability estimates.

443

444 To further explore unreliable heritability estimates of smaller regions, we combined the 4 smaller
445 regions that make up the orbitofrontal region to examine the effects of regional size on heritability
446 estimates of CT and SA using vertex-wise and ROI approach. The 4 regions that made up the
447 orbitofrontal region included: 1) Superior Frontal Gyrus: Orbital Part, 2) Inferior Frontal Gyrus: Orbital

448 Part, 3) Superior Frontal Gyrus: Medial Orbital, and 4) Middle Frontal Gyrus: Orbital Part (see Table
449 S7). In the vertex-wise approach SA heritability estimate for the total orbitofrontal region was 16% on
450 the left side with a slightly higher estimate on the right side, and the heritability estimates for CT was
451 20% for the left and similar pattern was seen on the right. The estimates of the combined region for both
452 CT and SA were very similar to the smaller individual regions such as the left and right inferior frontal
453 gyrus. In contrast, within the ROI approach, heritability estimates for both SA and CT were higher for
454 the combined areas of the orbitofrontal region compared to the individual regions such as the superior
455 frontal gyrus: medial orbital. In the ROI approach, SA of the total orbitofrontal region had heritability
456 estimates of 33% left with similar estimate on the right side, and heritability estimate of CT was 43%
457 left with a slightly lower estimate on the right side. Furthermore, in the ROI approach the heritability
458 confidence intervals included 0 for the individual regions of the orbitofrontal region, however when the
459 four regions were combined the confidence intervals showed a narrower range and did not include 0
460 (Table S7). The results suggest that combining smaller regions may result in more reliable heritability
461 estimates compared to individual smaller regions in which heritability of 0 are seen, particularly in the
462 ROI approach. This supports the idea that defining boundaries of smaller regions is difficult compared to
463 larger regions which can result in heritability estimates that are not reliable or are not biologically
464 plausible.

465

466 **In previous work, Eyler et al., (2012) also explored regional size and differences between**
467 **heritability estimates of ROI and vertex-wise approaches.** Eyler et al., (2012) examined heritability
468 estimates in a ratio form which was ROI heritability estimate over vertex-wise heritability estimate of a
469 region ($h^2_{ROI}/h^2_{vertex-wise}$). They plotted the ratio against the size of the ROI (measured in vertices)
470 and the line of best fit showed greater difference (low ratio) in heritability estimates between both
471 approaches in smaller regions compared to larger ROI regions where similar heritability estimates were
472 observed (ratio closer to 1). Similar observations were seen in our study, for example using the ratio
473 equation the left precentral gyrus region which had 1192 vertices had a ratio of 0.78 for CT and 0.68 for
474 SA, however the ratio was lower in smaller regions, such as the left supramarginal gyrus which has half
475 the number of vertices (564 vertices, ratio CT = 0.61, ratio SA= 0.42). **The sensitivity analysis of the**
476 **orbitofrontal region in our study along with the ratio quantification by Eyler et al., (2012), suggest**
477 **that changing the size of the regions to obtain the optimal size in order to get reliable heritability**
478 **estimates should be considered, specifically in the ROI approach.** Furthermore, by definition
479 combining regions will lead to higher heritability estimates compared to smaller regions. For example,
480 heritability of mean CT or total brain volume will always be higher than a regional measure. Further

481 research needs to be done to properly address the regional size effect on heritability estimates which
482 would require a well-designed systematic approach in varying regional sizes to find reliable heritability
483 estimates.

484

485 In spatial smoothing, target signals are averaged with neighbouring signals; therefore anatomical
486 boundaries of a region are blurred based on the spatial correlation between target and neighbouring
487 signals. Defining boundaries of smaller regions becomes harder based on the interference of
488 neighbouring signals during spatial smoothing, making it difficult to obtain accurate estimates of SA. In
489 this work, a larger spatial smoothing kernel was used for SA (40 mm) compared to CT (20 mm).
490 Therefore the SA smoothing kernel incorporates greater amount of neighbouring signal which can
491 interfere with target signals when defining smaller regions compared to the smoothing kernel used for
492 CT. We chose these values as they are the values most commonly used in MRI studies that employ
493 CIVET (Lax et al., 2013; Lyttelton et al., 2009; Sussman et al., 2016). Nonetheless, we do acknowledge
494 that larger smoothing kernels incorporate a greater number of neighbouring vertices, which may
495 interfere with the target signal at the vertex-level. In an exploratory analysis we examined the effect of
496 multiple smoothing kernels for SA (20mm, 10mm FWHM) and CT (5mm, 10mm FWHM) on
497 heritability estimates in a vertex-wise approach. Supplementary section: Sensitivity Analysis (see Inline
498 Supplementary Table S9), shows heritability estimates for each reduced smoothing kernel. Overall,
499 heritability estimates were similar between original smoothing kernel value and decreased kernel values.
500 For example the right inferior parietal (supramarginal and angular gyri) and both the left and right
501 parahippocampal gyrus had similar estimates particularly seen in SA compared to CT. Interestingly, a
502 trend was observed where larger the kernel value, greater the heritability estimates and smaller the
503 kernel value the lower the heritability estimates. Future studies should examine the influence of
504 smoothing kernel on heritability estimates in a systematic approach using a spectrum of different
505 smoothing kernels, this would add value to the imaging-genetics research field. Throughout the
506 discussion we have addressed some of the shortcomings of image processing; however there are also
507 limitations with the HCP sample. The sample is relatively young with an age group of 22-37 that does
508 not encompass the entire lifespan. Furthermore, information of intrauterine environment or pre and post
509 complication for twins and non-twin siblings in our study is not given which can influence
510 neuroanatomical measures affecting heritability estimates (Buckler and Green, 2004; Peterson et al.,
511 2000).

512

513 Similar heritability estimates between our study and Eyer's et al., 2012 study are observed throughout
514 different regions of the brain. For example, Eyer et al., 2012 reported heritability estimates of CT in the
515 fusiform gyrus region to be 40% (left) and 29% (right) in the vertex-wise approach compared to the ROI
516 approach which was 35% (left) and 44% (right). We showed slightly lower estimates using the vertex-
517 wise approach (24% left and 28% right) and similar results in the ROI approach (33% left and 47%
518 right). However, there were differences in heritability estimates which can be due to the demographics
519 of the sample and the type of imaging pipeline used. In our study, the CIVET pipeline was used to
520 measure CT and SA, whereas other heritability studies have used FreeSurfer (Docherty et al., 2015;
521 Eyer et al., 2012; Panizzon et al., 2009; Winkler et al., 2010). CIVET uses a skeleton mesh model base
522 and FreeSurfer uses a deformation of the inner surface model base. A one-to-one comparison between
523 FreeSurfer and CIVET-CLASP (slightly different from the CIVET version used in this study) on CT has
524 been done, and FreeSurfer CT measures were lower by one third compared to CIVET-CLASP (Redolfi
525 et al., 2015). This study also reported that CIVET-CLASP is more prone to topological errors whereas
526 FreeSurfer is more prone to geometric inaccuracies when forming the 3D mesh (Redolfi et al., 2015).
527 Both types of errors can influence the true estimate of CT and SA. Interestingly, in FreeSurfer the total
528 vertices mapped to the brain were 327,680 compared to our study which consisted of 81,924 vertices. As
529 a result, on a regional level, the number of vertices within a region is greater in FreeSurfer than CIVET
530 which may result in different overall averages of regional CT and SA between both pipelines, therefore
531 influencing overall regional heritability estimates. A comparison of results is difficult across CIVET and
532 FreeSurfer when different atlases are being used to define regions across the brain within the ROI
533 approach. As a supplementary analysis we selected 16 regions that were similar between CIVET and
534 FreeSurfer to compare heritability estimates. Results are seen in Supplementary Section: Sensitivity
535 Analysis (see Inline Supplementary Table S10). Many of the regions showed similar heritability
536 estimates with a difference of less than 10% between estimates, such as the parahippocampal gyrus and
537 posterior cingulate gyrus. However there were extreme differences in heritability estimates in some
538 regions, such as the superior temporal gyrus. Based on differences in imaging pipelines, a one-to-one
539 comparison of results is difficult since different atlases are being used, with different numbers of
540 vertices within each region to define the boundaries. This can influence CT and SA measures which in
541 turn influences heritability estimates between the different imaging pipelines. Therefore, a systematic
542 comparison study using same sample, same MRI resolution scans and atlases would benefit the imaging-
543 genetics field by showing the reliability and reproducibility of heritability estimates within different
544 imaging pipelines.

545

546 There are several studies that examine heritability estimates of neuroanatomical measures of the cortex
547 (Eyler et al., 2012; Ge et al., 2016; Patel et al., 2017; Winkler et al., 2010). For example, Winkler et al.,
548 2009, uses an extended family pedigree design in a ROI approach to examine the relationship between
549 regional grey matter volume, CT and SA measures and their heritability estimates. However, in our
550 study we focused on heritability estimates using both ROI and vertex-wise approaches and examine the
551 impact of input choice on downstream heritability estimates. In addition, we take advantage of a larger
552 sample size using the HCP dataset of twin and non-twin first degree related siblings. We believe it is
553 important to report heritable estimates using the publically available HCP dataset, which has not been
554 done before on CT and SA measures. We are aware of two studies that uses the HCP dataset to calculate
555 heritability estimates on different structural neuroanatomical measures. A study done by our group used
556 the 500 subject release from the HCP in an univariate model determining if heritability of hippocampal
557 subfields volumes were influenced by global measures such as total brain volume (TBV) and ipsilateral
558 hippocampal volume. Furthermore, a bivariate model was used to investigate the shared heritability and
559 genetic correlation of the subfield volumes with TBV and ipsilateral hippocampal volume (Patel et al.,
560 2017). A second study by Ge et al, (2016) used the HCP dataset as a replication set to calculate
561 heritability of volume and shape of subcortical structures (Ge et al., 2016). However, in our current
562 study we focused on heritability of SA and CT of all cortical regions, instead of volume and shape of
563 subcortical structures. Furthermore, our study had a larger sample size of 757 for heritability analysis on
564 HCP data compared to Ge et al., 2016 and Patel et al., 2017. We are not aware of any heritability
565 estimates released from the HCP using the FreeSurfer output for CT and SA. Furthermore, the main
566 focus and novelty of our study was to investigate why heritability estimates fail within the model when
567 we examine smaller regions, which has not been previously done.

568

569 5. CONCLUSION

570 In our study we used a univariate model to investigate the unique heritability estimates of CT and SA
571 within a young healthy population of male and female twins along with non-twin siblings. We have
572 shown that global structures such as total brain SA and average brain CT influence these regional
573 measures within the brain using both vertex-wise and ROI approaches. The heritability estimates we
574 produced in our study for CT and SA can be used by other researchers in choosing quantitative
575 phenotypes in imaging-genetics studies. CT and SA measures are less reliable and less accurate in
576 smaller regions compared to larger regions within the brain. This can cause the heritability model to fail
577 when the assumption that MZ twin correlation of a trait should be equal to or greater than DZ twins is
578 not met, resulting in heritability estimates of zero. Comparison studies focusing on reliability of
579 heritability estimates on smaller structures between different imaging pipelines can aid in capturing
580 accurate heritability estimates of brain regions that are difficult to define from imaging scans. Therefore,
581 it is important to identify which approach is best suited based on the research hypothesis and the size of
582 the regions being investigated in heritability analysis. Understanding the genetic variation of CT and SA
583 at a vertex and regional level through heritability is important in order to establish quantitative
584 phenotypes. These phenotypes can be used in understanding neurophysiological, neurodevelopmental
585 and neurodegenerative diseases in larger scale imaging genetics studies such as the ENIGMA
586 consortium (Stein et al., 2012; Thompson et al., 2014).

587

588 6. ACKNOWLEDGMENTS

589 Data were provided [in part] by the Human Connectome Project, WU-Minn Consortium (Principal
590 Investigators: David Van Essen and Kamil Ugurbil; 1U54MH091657) funded by the 16 NIH Institutes
591 and Centers that support the NIH Blueprint for Neuroscience Research; and by the McDonnell Center
592 for Systems Neuroscience at Washington University. Computations were performed on the gpc
593 supercomputer at the SciNet HPC Consortium (Loken et al., 2010). SciNet is funded by: the Canada
594 Foundation for Innovation under the auspices of Compute Canada; the Government of Ontario; Ontario
595 Research Fund - Research Excellence; and the University of Toronto. MMC is funded by the National
596 Sciences and Engineering Research Council, Canadian Institutes for Health Research, Weston Brain
597 Institute, Michael J. Fox Foundation for Parkinson's Research, Alzheimer's Society, and Brain Canada.
598 JK holds the Joanne Murphy Professorship in Behavioral Science and is also funded by the Canadian
599 Institutes for Health Research. SP is funded by the Cadsby Foundation and Canadian Institutes for
600 Health Research. The authors report no conflict of interest.

601
602

References

- 603 Ad-Dab'bagh, Y., Lyttelton, O., Muehlboeck, J., *et al.*, 2006. The CIVET image-processing environment: a fully
604 automated comprehensive pipeline for anatomical neuroimaging research. Proceedings of the 12th annual
605 meeting of the organization for human brain mapping. Florence, Italy, p. 2266
- 606 Baare, W.F., Hulshoff Pol, H.E., Boomsma, D.I., *et al.*, 2001. Quantitative genetic modeling of variation in human
607 brain morphology. *Cerebral cortex* 11, 816-824.
- 608 Barry, D.S., Pakan, J.M., McDermott, K.W., 2014. Radial glial cells: key organisers in CNS development. *Int J*
609 *Biochem Cell Biol* 46, 76-79. doi:10.1016/j.biocel.2013.11.013
- 610 Bollen, K.A., 1989. A new incremental fit index for general structural equation models. *Sociological Methods &*
611 *Research* 17, 303-316.
- 612 Buckler, J.M., Green, M., 2004. A comparison of the early growth of twins and singletons. *Annals of human*
613 *biology* 31, 311-332. doi:10.1080/03014460410001670120
- 614 Collins, D.L., Neelin, P., Peters, T.M., *et al.*, 1994. Automatic 3D intersubject registration of MR volumetric data
615 in standardized Talairach space. *Journal of computer assisted tomography* 18, 192-205.
- 616 Diamantopoulos, A., Siguaw, J.A., Siguaw, J.A., 2000. *Introducing LISREL: A guide for the uninitiated*. Sage.
- 617 Docherty, A.R., Sawyers, C.K., Panizzon, M.S., *et al.*, 2015. Genetic network properties of the human cortex
618 based on regional thickness and surface area measures. *Frontiers in human neuroscience* 9, 440.
619 doi:10.3389/fnhum.2015.00440
- 620 Eyler, L.T., Chen, C.H., Panizzon, M.S., *et al.*, 2012. A comparison of heritability maps of cortical surface area and
621 thickness and the influence of adjustment for whole brain measures: a magnetic resonance imaging twin study.
622 *Twin Res Hum Genet* 15, 304-314. doi:10.1017/thg.2012.3
- 623 Ge, T., Nichols, T.E., Lee, P.H., *et al.*, 2015. Massively expedited genome-wide heritability analysis (MEGHA).
624 *Proceedings of the National Academy of Sciences of the United States of America* 112, 2479-2484.
625 doi:10.1073/pnas.1415603112
- 626 Ge, T., Reuter, M., Winkler, A.M., *et al.*, 2016. Multidimensional heritability analysis of neuroanatomical shape.
627 *Nat Commun* 7, 13291. doi:10.1038/ncomms13291
- 628 Geschwind, D.H., Miller, B.L., DeCarli, C., *et al.*, 2002. Heritability of lobar brain volumes in twins supports
629 genetic models of cerebral laterality and handedness. *Proceedings of the National Academy of Sciences of the*
630 *United States of America* 99, 3176-3181. doi:10.1073/pnas.052494999
- 631 Glasser, M.F., Goyal, M.S., Preuss, T.M., *et al.*, 2014. Trends and properties of human cerebral cortex:
632 correlations with cortical myelin content. *Neuroimage* 93 Pt 2, 165-175. doi:10.1016/j.neuroimage.2013.03.060
- 633 Glasser, M.F., Sotiropoulos, S.N., Wilson, J.A., *et al.*, 2013. The minimal preprocessing pipelines for the Human
634 Connectome Project. *Neuroimage* 80, 105-124. doi:10.1016/j.neuroimage.2013.04.127
- 635 Jacquard, A., 1983. Heritability: one word, three concepts. *Biometrics* 39, 465-477.
- 636 Kaas, J.H., 2008. The evolution of the complex sensory and motor systems of the human brain. *Brain Res Bull* 75,
637 384-390. doi:10.1016/j.brainresbull.2007.10.009
- 638 Kim, J.S., Singh, V., Lee, J.K., *et al.*, 2005. Automated 3-D extraction and evaluation of the inner and outer cortical
639 surfaces using a Laplacian map and partial volume effect classification. *Neuroimage* 27, 210-221.
640 doi:10.1016/j.neuroimage.2005.03.036
- 641 Kremen, W.S., Prom-Wormley, E., Panizzon, M.S., *et al.*, 2010. Genetic and environmental influences on the size
642 of specific brain regions in midlife: the VETSA MRI study. *Neuroimage* 49, 1213-1223.
643 doi:10.1016/j.neuroimage.2009.09.043
- 644 Kretschmann, H.J., Schleicher, A., Wingert, F., *et al.*, 1979. Human brain growth in the 19th and 20th century.
645 *Journal of the neurological sciences* 40, 169-188.
- 646 Lax, I.D., Duerden, E.G., Lin, S.Y., *et al.*, 2013. Neuroanatomical consequences of very preterm birth in middle
647 childhood. *Brain Struct Funct* 218, 575-585. doi:10.1007/s00429-012-0417-2

- 648 Lenroot, R.K., Giedd, J.N., 2008. The changing impact of genes and environment on brain development during
649 childhood and adolescence: initial findings from a neuroimaging study of pediatric twins. *Dev Psychopathol* 20,
650 1161-1175. doi:10.1017/S0954579408000552
- 651 Lerch, J.P., Evans, A.C., 2005. Cortical thickness analysis examined through power analysis and a population
652 simulation. *Neuroimage* 24, 163-173. doi:10.1016/j.neuroimage.2004.07.045
- 653 Loken, C., Gruner, D., Groer, L., *et al.*, 2010. SciNet: lessons learned from building a power-efficient top-20
654 system and data centre. *Journal of Physics: Conference Series*. IOP Publishing, p. 012026
- 655 Lyttelton, O., Boucher, M., Robbins, S., *et al.*, 2007. An unbiased iterative group registration template for cortical
656 surface analysis. *Neuroimage* 34, 1535-1544. doi:10.1016/j.neuroimage.2006.10.041
- 657 Lyttelton, O.C., Karama, S., Ad-Dab'bagh, Y., *et al.*, 2009. Positional and surface area asymmetry of the human
658 cerebral cortex. *Neuroimage* 46, 895-903. doi:10.1016/j.neuroimage.2009.03.063
- 659 MacDonald, D., Kabani, N., Avis, D., *et al.*, 2000. Automated 3-D extraction of inner and outer surfaces of
660 cerebral cortex from MRI. *Neuroimage* 12, 340-356. doi:10.1006/nimg.1999.0534
- 661 Neale, M.C., Hunter, M.D., Pritikin, J.N., *et al.*, 2016. OpenMx 2.0: Extended Structural Equation and Statistical
662 Modeling. *Psychometrika* 81, 535-549. doi:10.1007/s11336-014-9435-8
- 663 Neale, M.C., Miller, M.B., 1997. The use of likelihood-based confidence intervals in genetic models. *Behavior*
664 *genetics* 27, 113-120.
- 665 Noctor, S.C., Flint, A.C., Weissman, T.A., *et al.*, 2001. Neurons derived from radial glial cells establish radial units
666 in neocortex. *Nature* 409, 714-720. doi:10.1038/35055553
- 667 Noctor, S.C., Martinez-Cerdeno, V., Ivic, L., *et al.*, 2004. Cortical neurons arise in symmetric and asymmetric
668 division zones and migrate through specific phases. *Nature neuroscience* 7, 136-144. doi:10.1038/nn1172
- 669 Oldfield, R.C., 1971. The assessment and analysis of handedness: the Edinburgh inventory. *Neuropsychologia* 9,
670 97-113.
- 671 Panizzon, M.S., Fennema-Notestine, C., Eyler, L.T., *et al.*, 2009. Distinct genetic influences on cortical surface
672 area and cortical thickness. *Cerebral cortex* 19, 2728-2735. doi:10.1093/cercor/bhp026
- 673 Patel, S., Park, M.T.M., Devenyi, G.A., *et al.*, 2017. Heritability of hippocampal subfield volumes using a twin and
674 non-twin siblings design. *Hum Brain Mapp* 38, 4337-4352. doi:10.1002/hbm.23654
- 675 Pennington, B.F., Filipek, P.A., Lefly, D., *et al.*, 2000. A twin MRI study of size variations in human brain. *Journal*
676 *of cognitive neuroscience* 12, 223-232.
- 677 Peterson, B.S., Vohr, B., Staib, L.H., *et al.*, 2000. Regional brain volume abnormalities and long-term cognitive
678 outcome in preterm infants. *JAMA* 284, 1939-1947.
- 679 Plomin, R., Willerman, L., Loehlin, J.C., 1976. Resemblance in appearance and the equal environments
680 assumption in twin studies of personality traits. *Behavior genetics* 6, 43-52.
- 681 Pontious, A., Kowalczyk, T., Englund, C., *et al.*, 2008. Role of intermediate progenitor cells in cerebral cortex
682 development. *Dev Neurosci* 30, 24-32. doi:10.1159/000109848
- 683 Posthuma, D., Boomsma, D.I., 2000. A note on the statistical power in extended twin designs. *Behavior genetics*
684 30, 147-158.
- 685 Rakic, P., 1988. Specification of cerebral cortical areas. *Science* 241, 170-176.
- 686 Rakic, P., 2007. The radial edifice of cortical architecture: from neuronal silhouettes to genetic engineering. *Brain*
687 *research reviews* 55, 204-219. doi:10.1016/j.brainresrev.2007.02.010
- 688 Rakic, P., 2009. Evolution of the neocortex: a perspective from developmental biology. *Nat Rev Neurosci* 10,
689 724-735. doi:10.1038/nrn2719
- 690 Redolfi, A., Manset, D., Barkhof, F., *et al.*, 2015. Head-to-head comparison of two popular cortical thickness
691 extraction algorithms: a cross-sectional and longitudinal study. *PloS one* 10, e0117692.
692 doi:10.1371/journal.pone.0117692
- 693 Reinartz, W., Haenlein, M., Henseler, J., 2009. An empirical comparison of the efficacy of covariance-based and
694 variance-based SEM. *International Journal of research in Marketing* 26, 332-344.

- 695 Rimol, L.M., Panizzon, M.S., Fennema-Notestine, C., *et al.*, 2010. Cortical thickness is influenced by regionally
696 specific genetic factors. *Biological psychiatry* 67, 493-499. doi:10.1016/j.biopsych.2009.09.032
- 697 Stein, J.L., Medland, S.E., Vasquez, A.A., *et al.*, 2012. Identification of common variants associated with human
698 hippocampal and intracranial volumes. *Nature genetics* 44, 552-561. doi:10.1038/ng.2250
- 699 Steindler, D.A., 1993. Glial boundaries in the developing nervous system. *Annu Rev Neurosci* 16, 445-470.
700 doi:10.1146/annurev.ne.16.030193.002305
- 701 Sussman, D., Leung, R.C., Chakravarty, M.M., *et al.*, 2016. Developing human brain: age-related changes in
702 cortical, subcortical, and cerebellar anatomy. *Brain Behav* 6, e00457. doi:10.1002/brb3.457
- 703 Swaab, D.F., Hofman, M.A., 1984. Sexual differentiation of the human brain. A historical perspective. *Progress in*
704 *brain research* 61, 361-374. doi:10.1016/S0079-6123(08)64447-7
- 705 Thompson, P.M., Cannon, T.D., Narr, K.L., *et al.*, 2001a. Genetic influences on brain structure. *Nature*
706 *neuroscience* 4, 1253-1258. doi:10.1038/nn758
- 707 Thompson, P.M., Stein, J.L., Medland, S.E., *et al.*, 2014. The ENIGMA Consortium: large-scale collaborative
708 analyses of neuroimaging and genetic data. *Brain imaging and behavior* 8, 153-182. doi:10.1007/s11682-013-
709 9269-5
- 710 Thompson, P.M., Vidal, C., Giedd, J.N., *et al.*, 2001b. Mapping adolescent brain change reveals dynamic wave of
711 accelerated gray matter loss in very early-onset schizophrenia. *Proceedings of the National Academy of Sciences*
712 *of the United States of America* 98, 11650-11655. doi:10.1073/pnas.201243998
- 713 Tzourio-Mazoyer, N., Landeau, B., Papathanassiou, D., *et al.*, 2002. Automated anatomical labeling of activations
714 in SPM using a macroscopic anatomical parcellation of the MNI MRI single-subject brain. *Neuroimage* 15, 273-
715 289. doi:10.1006/nimg.2001.0978
- 716 Van Essen, D.C., Smith, S.M., Barch, D.M., *et al.*, 2013. The WU-Minn Human Connectome Project: an overview.
717 *Neuroimage* 80, 62-79. doi:10.1016/j.neuroimage.2013.05.041
- 718 Van Essen, D.C., Ugurbil, K., Auerbach, E., *et al.*, 2012. The Human Connectome Project: a data acquisition
719 perspective. *Neuroimage* 62, 2222-2231. doi:10.1016/j.neuroimage.2012.02.018
- 720 Winkler, A.M., Kochunov, P., Blangero, J., *et al.*, 2010. Cortical thickness or grey matter volume? The importance
721 of selecting the phenotype for imaging genetics studies. *Neuroimage* 53, 1135-1146.
722 doi:10.1016/j.neuroimage.2009.12.028

723 TABLES

724

725 **TABLE 3. Heritability estimates (H^2) for cortical thickness and surface area from vertex-wise and**
 726 **ROI approach along with number of vertices within each region. Heritability estimates are**
 727 **defined in left and right regions from the AAL atlas. Partially adjusted values are controlled for**
 728 **sex and age. Completely adjusted values are controlled for sex, age and ipsilateral average brain**
 729 **cortical thickness or ipsilateral total surface area.**

Region	Number of vertices	Mean Cortical Thickness				Total Surface Area			
		Partially adjusted		Completely adjusted		Partially adjusted		Completely adjusted	
		Vertex	ROI	Vertex	ROI	Vertex	ROI	Vertex	ROI
Frontal Lobe									
Precentral Gyrus-Left	1192	33%	42%	22%	35%	39%	57%	20%	35%
Precentral Gyrus-Right	1183	38%	59%	21%	32%	47%	50%	21%	22%
Superior Frontal Gyrus: Dorsolateral-Left	1598	29%	45%	24%	25%	35%	48%	17%	29%
Superior Frontal Gyrus: Dorsolateral-Right	1394	39%	60%	25%	32%	40%	51%	13%	28%
Superior Frontal Gyrus: Orbital Part-Left	903	35%	47%	29%	42%	47%	39%	24%	17%
Superior Frontal Gyrus: Orbital Part-Right	848	37%	54%	30%	45%	48%	20%	19%	2%
Superior Frontal Gyrus: Medial-Left	1280	36%	55%	28%	45%	38%	45%	13%	22%
Superior Frontal Gyrus: Medial-Right	781	48%	67%	30%	42%	44%	35%	13%	8%
Superior Frontal Gyrus: Medial Orbital-Left	409	20%	0%	22%	0%	30%	4%	10%	0%
Superior Frontal Gyrus: Medial Orbital-Right	403	37%	55%	22%	32%	52%	27%	20%	8%
Middle Frontal Gyrus-Left	1823	30%	54%	22%	53%	39%	56%	17%	25%
Middle Frontal Gyrus-Right	2112	34%	66%	17%	34%	48%	68%	18%	36%
Middle Frontal Gyrus: Orbital Part-Left	350	19%	28%	14%	16%	46%	0%	30%	1%
Middle Frontal Gyrus: Orbital Part-Right	410	35%	53%	26%	44%	52%	30%	17%	6%
Inferior Frontal Gyrus: Opercular Part-Left	520	41%	49%	23%	22%	56%	22%	25%	2%
Inferior Frontal Gyrus: Opercular Part-Right	516	40%	50%	28%	31%	50%	44%	29%	34%
Inferior Frontal Gyrus: Orbital Part-Left	965	22%	26%	19%	24%	28%	30%	18%	19%
Inferior Frontal Gyrus: Orbital Part-Right	973	31%	38%	24%	41%	42%	41%	27%	30%
Inferior Frontal Gyrus: Triangular Part-Left	782	44%	61%	30%	44%	34%	22%	19%	23%

Region	Number of vertices	Mean Cortical Thickness				Total Surface Area			
		Partially adjusted		Completely adjusted		Partially adjusted		Completely adjusted	
		Vertex	ROI	Vertex	ROI	Vertex	ROI	Vertex	ROI
Inferior Frontal Gyrus: Triangular Part-Right	819	38%	67%	27%	49%	44%	12%	25%	7%
Paracentral Lobule-Left	842	30%	32%	29%	38%	27%	26%	20%	19%
Paracentral Lobule-Right	644	32%	29%	32%	41%	33%	27%	20%	9%
Rolandic Operculum-Left	445	51%	64%	23%	30%	55%	37%	28%	24%
Rolandic Operculum-Right	456	54%	66%	26%	22%	42%	15%	17%	0%
Supplementary Motor Area-Left	916	39%	58%	29%	49%	44%	37%	18%	17%
Supplementary Motor Area-Right	1006	49%	69%	30%	41%	44%	40%	27%	29%
Olfactory Cortex-Left	183	19%	15%	30%	34%	58%	35%	40%	31%
Olfactory Cortex-Right	132	22%	16%	17%	9%	46%	0%	24%	0%
Gyrus Rectus-Left	502	28%	21%	32%	33%	44%	20%	25%	15%
Gyrus Rectus-Right	481	42%	57%	29%	42%	51%	38%	28%	29%
Parietal Lobe									
Postcentral Gyrus-Left	1693	33%	43%	24%	53%	38%	52%	15%	22%
Postcentral Gyrus-Right	1617	39%	59%	27%	31%	41%	44%	22%	18%
Superior Parietal Gyrus-Left	1366	44%	53%	31%	56%	51%	29%	31%	18%
Superior Parietal Gyrus-Right	1448	36%	51%	26%	47%	46%	42%	23%	18%
Inferior Parietal: Supramarginal and Angular Gyri-Left	670	25%	27%	15%	34%	48%	34%	24%	22%
Inferior Parietal: Supramarginal and Angular Gyri-Right	388	33%	40%	12%	15%	29%	12%	6%	4%
Supramarginal Gyrus-Left	564	44%	71%	18%	23%	38%	16%	16%	8%
Supramarginal Gyrus-Right	805	42%	59%	22%	28%	38%	30%	26%	27%
Angular Gyrus-Left	633	31%	49%	14%	31%	51%	29%	37%	19%
Angular Gyrus-Right	636	27%	49%	17%	29%	44%	39%	21%	27%
Precuneus-Left	2268	33%	50%	25%	42%	64%	71%	41%	44%
Precuneus-Right	2271	41%	62%	25%	29%	62%	68%	43%	48%
Temporal Lobe									
Superior Temporal Gyrus-Left	1531	35%	48%	24%	6%	36%	48%	22%	38%
Superior Temporal Gyrus-Right	1789	42%	66%	25%	25%	33%	20%	27%	8%
Temporal Pole: Superior Temporal Gyrus-Left	563	27%	28%	27%	30%	32%	14%	15%	7%
Temporal Pole: Superior Temporal Gyrus-Right	628	34%	40%	30%	35%	46%	45%	32%	25%

Region	Number of vertices	Mean Cortical Thickness				Total Surface Area			
		Partially adjusted		Completely adjusted		Partially adjusted		Completely adjusted	
		Vertex	ROI	Vertex	ROI	Vertex	ROI	Vertex	ROI
Middle Temporal Gyrus-Left	2076	31%	52%	17%	48%	33%	38%	24%	27%
Middle Temporal Gyrus-Right	1813	36%	59%	24%	45%	37%	59%	24%	33%
Temporal Pole: Middle Temporal Gyrus-Left	169	25%	36%	24%	32%	28%	15%	15%	17%
Temporal Pole: Middle Temporal Gyrus-Right	224	40%	49%	33%	42%	25%	0%	18%	0%
Inferior Temporal Gyrus-Left	975	28%	52%	19%	39%	52%	53%	28%	30%
Inferior Temporal Gyrus-Right	1086	31%	65%	20%	44%	41%	45%	25%	24%
Parahippocampal Gyrus-Left	1130	41%	54%	35%	43%	51%	45%	28%	31%
Parahippocampal Gyrus-Right	1126	39%	45%	36%	42%	47%	43%	31%	31%
Fusiform Gyrus-Left	1169	33%	45%	24%	33%	45%	9%	16%	2%
Fusiform Gyrus-Right	1149	37%	70%	28%	47%	49%	43%	23%	26%
Heschl Gyrus-Left	271	40%	41%	28%	27%	42%	0%	23%	0%
Heschl Gyrus-Right	252	51%	62%	34%	38%	31%	0%	17%	0%
Occipital Lobe									
Superior Occipital Gyrus-Left	841	45%	45%	37%	56%	45%	29%	31%	21%
Superior Occipital Gyrus-Right	796	35%	48%	24%	43%	48%	39%	28%	25%
Middle Occipital Gyrus-Left	1685	36%	64%	17%	38%	34%	19%	24%	15%
Middle Occipital Gyrus-Right	1374	26%	43%	14%	18%	41%	31%	21%	13%
Inferior Occipital Gyrus-Left	495	32%	27%	16%	0%	43%	0%	28%	8%
Inferior Occipital Gyrus-Right	630	26%	30%	17%	16%	47%	17%	25%	11%
Calcarine Fissure and Surrounding Cortex-Left	1102	28%	45%	24%	45%	60%	51%	51%	41%
Calcarine Fissure and Surrounding Cortex-Right	1086	31%	49%	25%	56%	61%	56%	48%	44%
Cuneus-Left	1309	36%	48%	28%	53%	63%	50%	49%	40%
Cuneus-Right	1325	38%	55%	29%	51%	58%	33%	46%	29%
Lingual Gyrus-Left	964	30%	38%	27%	43%	50%	37%	34%	31%
Lingual Gyrus-Right	949	32%	51%	24%	41%	56%	44%	39%	39%
Insula and Cingulate Gyri									
Insula-Left	1042	40%	37%	34%	42%	36%	55%	17%	37%
Insula-Right	1077	35%	37%	31%	41%	22%	29%	20%	35%
Anterior Cingulate and Paracingulate Gyri-Left	662	17%	15%	17%	24%	43%	1%	15%	0%
Anterior Cingulate and Paracingulate Gyri-Right	1076	37%	56%	26%	37%	47%	12%	23%	0%
Median Cingulate and Paracingulate Gyri-Left	1070	41%	62%	26%	52%	48%	20%	25%	20%

Region	Number of vertices	Mean Cortical Thickness				Total Surface Area			
		Partially adjusted		Completely adjusted		Partially adjusted		Completely adjusted	
		Vertex	ROI	Vertex	ROI	Vertex	ROI	Vertex	ROI
Median Cingulate and Paracingulate Gyri-Right	1258	45%	64%	31%	59%	53%	37%	27%	3%
Posterior Cingulate Gyrus-Left	328	35%	36%	38%	49%	68%	22%	45%	14%
Posterior Cingulate Gyrus-Right	325	48%	50%	42%	52%	65%	42%	45%	32%
Whole Brain									
Brain Hemisphere - Left		-	46%	-	-	-	75%	-	-
Brain Hemisphere - Right		-	67%	-	-	-	73%	-	-

730